J. Fluid Mech. (1981), *vol.* 110, *pp.* 297–334
Printed in Great Britain

The amplitude equation near the convective threshold: application to time-dependent heating experiments

By GUENTER AHLERS,

Bell Laboratories, Murray Hill, New Jersey 07974 and Department of Physics, University of California, Santa Barbara, California 93106

M. C. CROSS, P. C. HOHENBERG AND S. SAFRAN

Bell Laboratories, Murray Hill, New Jersey 07974

(Received 15 May 1980 and in revised form 9 December 1980)

High-resolution measurements have been performed of the convective heat current as a function of time when a Rayleigh–Bénard cell is swept through its threshold with a specified time-dependent heat input. The results are interpreted in terms of the amplitude equation which exactly describes the slow variations in space and time of hydrodynamic quantities near the threshold. A phenomenological forcing field is added to this equation, and its form and magnitude are fitted to the onset time of the convective heat current. A deterministic model in which the field is an adjustable constant yields a good fit to the data for both a step and a linear ramp in the heat input. An alternative stochastic model, in which the field is a Gaussian variable with zero mean and a white-noise spectrum, is adequate for the ramp experiments, but cannot fit the step data for any value of the mean-square field. The systematics of the field and onset time versus ramp rate are studied in both the deterministic and stochastic models, and attempts are made to interpret the field in terms of physical mechanisms. When the data for long times are analysed in terms of the amplitude equation, it is found that the state first excited at onset is not the roll pattern which is stable in steady state. Instead, the system goes first to an intermediate state, which we tentatively identify as a hexagonal configuration. The decay of this state is governed by a further adjustable field in the amplitude equation.

1. Introduction

The states of flow occurring near the onset of Rayleigh–Bénard convection can be described by an amplitude equation (Segel 1969; Newell & Whitehead 1969), which represents a considerable simplification of the full hydrodynamic equations (Schlüter, Lortz & Busse 1965; Busse 1978). Efforts to verify the predictions of the amplitude equation in a quantitative way have been primarily restricted to steady flows, although some information has also been obtained on the time scale of changes in the flow pattern (Wesfreid *et al.* 1978; Behringer & Ahlers 1977, 1982; Normand, Pomeau & Velarde 1977). A problem which has attracted some interest in the past is the dynamic onset of convection when a system is swept through the convective threshold by heating the bottom plate (Spangenberg & Rowland 1961; Foster 1965*a*, *b*, 1969; Davis 1971). It is natural to assume that, if the system remains near the threshold, its response should be describable by the amplitude equation, which is sufficiently simple to yield rather detailed quantitative predictions. This paper presents a set of such experiments in

which the response was determined as a function of time, by accurate measurements of the Nusselt number.

The amplitude equation of Segel, and Newell & Whitehead is a partial differential equation for an order parameter ψ, whose stationary value is zero in the conducting regime below the threshold (Rayleigh number R less than R_c). This conducting solution becomes unstable when $R > R_c$, but it remains a solution of the *homogeneous* amplitude equation. In order to describe the dynamic process by which a non-zero ψ develops in the system, it is thus necessary to assume a finite value for ψ even below the threshold (Foster 1965*a*; Gollub & Freilich 1976). A convenient way to do this is to add to the amplitude equation an inhomogeneous term, whose form and magnitude will control the time scale for the onset of convection. The physical origin of such a term is rather difficult to elucidate in detail, though a number of possible mechanisms suggest themselves rather naturally, such as imperfections in the cell geometry (Kelly & Pal 1976), lateral heat flow (Daniels 1977; Hall & Walton 1977), and intrinsic fluctuation effects (Zaitsev & Shliomis 1970; Graham 1974; Swift & Hohenberg 1977). The last class of phenomena have been discussed theoretically in the recent literature, but have so far not been observed experimentally. We show below that the extremely small thermal fluctuations present in all fluids would lead to observable effects in the present dynamic experiments, if other effects leading to inhomogeneous terms could be suppressed. This is, however, not the case, so we have failed to detect thermal fluctuations of the theoretically predicted magnitude. A similar conclusion was reached by Sano & Sawada (1978).

Earlier experimental investigations of the dynamic onset of convection have been at best semi-quantitative, and have primarily focused on a determination of the onset time where convective patterns first appear (Spangenberg & Rowland 1961; Foster 1965*b*). Since the rate of heating in these experiments was high, the system reached a quasi-steady state of convection very far above the threshold, for which no simple description exists even in steady state. The theories which have been applied to this problem have therefore been restricted to linear stability analyses of the time-dependent situation, in order to determine the onset time (Morton 1957; Lick 1965; Foster 1965*a*; Robinson 1967; Homsy 1973; Wankat & Homsy 1977). The comparison between the theories and the above-mentioned experiments have been rather qualitative, and have only concerned the initial appearance of convection.

This work presents high-accuracy measurements of the full evolution of the heat current from the conducting state (Nusselt number $N = 1$), to the convecting state ($N > 1$). By limiting the heating to low amplitudes we are able to remain in the region of weak convection ($N - 1 \ll 1$), where the amplitude equation is valid. This permits a fully nonlinear analysis which includes both the onset time and the later stages of growth and saturation of the convective heat current. The calculations based on the amplitude equation can then be tested *quantitatively*.

In view of the uncertainties concerning the precise mechanism which triggers convection, we have used a phenomenological approach, in which an inhomogeneous forcing field is added to the amplitude equation, and the magnitude and form of this field are fitted to the data. The homogeneous part of the equation has no free parameters, however, since we have taken into account the finite lateral extent of the system, using the boundary conditions discussed by Daniels (1977) and Brown & Stewartson (1977). By studying the systematics of the forcing field, for a set of

experiments where the heat was applied either in a sudden step, or in a linear ramp with varying ramp rate, we are able to draw some conclusions on the mechanism which triggers convection, and also to test the validity of the amplitude equation. The main results of the present work are as follows.

(i) The overall predictions of the amplitude equation concerning the dependence of Nusselt number on cell geometry and Rayleigh number in steady state, as well as the basic time scale for changes in Nusselt number near the threshold, are quantitatively confirmed. Similar results have been obtained for the Taylor problem near onset by Gollub & Freilich (1976).

(ii) The convection pattern which is excited initially is not the one which eventually becomes stable in steady state. The system goes initially to an intermediate state which we analyse in terms of a *hexagon* structure, in contrast to the roll structure which occurs in steady state. A hexagon pattern has been predicted and observed in a somewhat similar situation in which both the upper and lower plates have time-varying temperatures, albeit at much higher ramp rates (Krishnamurti 1968*a*, *b*).

(iii) A *deterministic* model with a constant forcing field yields a good fit to the shape of the Nusselt number *vs.* time curve at onset. An extension of the model with two fields describes the further decay of the intermediate (hexagon) pattern to the stable (roll) configuration, for both steps and ramps in the heat input. The dependence of the field on ramp rate is roughly linear, with a *finite* intercept at zero ramp rate. This residual field which is not related to the time dependence of the heat input can be used to estimate the rounding of the N *vs.* R curve in steady state, in reasonable agreement with the independent experiments of Behringer & Ahlers (1982).

(iv) A *stochastic* forcing field with Gaussian white noise statistics was also used in the amplitude equation, in an attempt to model fluctuation effects. Approximate solutions of the ensuing nonlinear stochastic equation yielded a significantly worse fit to the N *vs.* t curves for the step experiments than the deterministic model. For the ramp experiments the stochastic and deterministic models fitted equally well. The magnitude of the noise necessary to obtain the correct onset time for either the step or the ramp, was larger than the thermal noise by a factor of 6×10^3. The noise amplitude fitted from dynamic experiments also yielded a rounding of the N *vs.* R curve which agreed with static experiments.

It must be stated, finally, that our conclusions concerning the spatial form of the convection pattern in the metastable and stable states must remain tentative, since the experiments only measure the overall Nusselt number, and give no direct information on the spatial configuration. It is entirely possible that more complicated patterns than the ones we considered are present in the cell, and lead to nearly the same Nusselt numbers. On the other hand the theory itself contains detailed information on spatial structure and it would be interesting to bring it to bear on accurate dynamic experiments using local probes (Bergé & Dubois 1974; Wesfreid *et al.* 1978; Gollub & Benson 1980; Libchaber & Maurer 1978).

The paper is divided into four sections. In § 2 the presently known information concerning the amplitude equation is summarized, including the effect of boundary conditions at the horizontal and lateral walls, and the influence of cell geometry (§§ 2.1, 2.2). A discussion is presented of the conditions under which the partial differential equation satisfied by $\psi(\mathbf{r}, t)$ can be replaced by an ordinary differential

equation for the amplitude $A(t)$ of a single mode (§ 2.3). The different forms used for the phenomenological forcing field are briefly discussed (§ 2.4). Section 3 describes the dynamic experiments and § 4 contains an analysis of the results. The model with a single roll pattern growing initially and saturating at long times is shown to disagree with the data (§ 4.2), and is replaced by one with a hexagon pattern followed by a stable roll pattern; this model fits the experiments with two adjustable field parameters (§ 4.3). The full partial differential equation is solved numerically for the growth of a roll pattern initially excited at the outer edge of the cell, and propagating into the interior (§ 4.4). The stochastic model is then considered and shown to disagree with the step data, but to agree rather well with the ramp experiments (§ 4.5). The systematics of the field values and onset times as a function of ramp rate and initial equilibration level are studied and compared with theoretical estimates (§ 4.6). Many of the detailed calculations are contained in appendixes A–D.

Preliminary accounts of parts of this work have been given by Ahlers (1978) and Ahlers & Hohenberg (1978).

2. The amplitude equation

In this section we shall summarize the available information on the amplitude equation, in a rather general context. The specific application to the time-dependent heating experiments will be discussed in § 4.

2.1. *Laterally infinite system*

For a system with free horizontal boundaries the amplitude equation was first derived from the hydrodynamic equations by Newell & Whitehead (1969) and by Segel (1969) (see also Joseph 1976; Normand *et al.* 1977). It describes the slow variations (in space and time) of velocities and temperature near the convective threshold $R = R_c^\infty$, in terms of an order parameter $\psi(\mathbf{r}, t)$, which is the projection of the hydrodynamic variables onto the slowest unstable mode of the system.

The equation involves only the two-dimensional horizontal direction $\mathbf{r}$, and it may conveniently be written in the form (Graham 1974; Swift & Hohenberg 1977)

$$\frac{\partial \psi(\mathbf{r}, t)}{\partial t} = -\frac{1}{\tau_0}\frac{\delta \tilde{\mathbf{F}}}{\delta \psi}, \tag{2.1}$$

$$\mathbf{F} = \int d^2r \{-\tfrac{1}{2}\epsilon\psi^2 + \tfrac{1}{4}g\psi^4 + \tfrac{1}{2}\tilde{\xi}_0^4[(\nabla^2 + q_0^2)\psi]^2\}, \tag{2.2}$$

where t is the time, q_0 is the critical wavevector, ψ is a *real* function and ϵ is given by

$$\epsilon = (R/R_c^\infty) - 1. \tag{2.3}$$

The quartic term has been written schematically as $g\psi^4$ in (2.2); in general it involves a non-local coupling between ψ values at different spatial points (see appendix A). The quantities τ_0, $\tilde{\xi}_0$, q_0 and g were evaluated by Newell & Whitehead for a system with free horizontal boundaries. For the rigid case, an amplitude equation of precisely the same form may be derived (Cross 1980), with different values for the parameters τ_0, R_c^∞, q_0, $\tilde{\xi}_0$ and g (Schlüter *et al.* 1965; Wesfreid *et al.* 1978; Behringer & Ahlers 1977) (see table 1). The normalization of ψ is chosen so that

$$S^{-1}\int d^2r\, \psi^2 = (N-1)\, R/R_c \equiv \mathcal{N}, \tag{2.4}$$

	Rigid boundary conditions		
		Value for $\sigma = 0{\cdot}78$	Free boundary conditions
R_c^∞	1707	—	$\frac{27\pi^4}{4}$
$q_0 d$	3·117	—	$\pi/\sqrt{2}$
τ_0^{-1}	$\frac{19{\cdot}65\sigma}{\sigma+0{\cdot}5117}$	11·87	$\left(\frac{3\pi^2}{2}\right)\frac{\sigma}{\sigma+1}$
ξ_0^2	0·148	—	$8/3\pi^2$
g	$0{\cdot}0083\sigma^{-2}-0{\cdot}0047\sigma^{-1}+0{\cdot}6995$	0·707	0·5
β	$\frac{0{\cdot}0893\sigma^{-2}+0{\cdot}0814\sigma^{-1}+0{\cdot}2913}{0{\cdot}0083\sigma^{-2}-0{\cdot}0047\sigma^{-1}+0{\cdot}6995}$	0·767	$0{\cdot}5676+0{\cdot}137\sigma^{-1}+0{\cdot}2126\sigma^{-2}$

TABLE 1

where N is the Nusselt number, and S is the area of the layer. The symbol $\mathscr{N}$ will be used throughout to denote the dimensionless convective heat current. The hydrodynamic variables (velocities and temperature) are expressible in terms of ψ, as spelled out in appendix A.

As it is written in (2.2), the amplitude equation contains terms with fourth powers of the gradient, which are in general outside the domain of validity of the lowest-order gradient expansion. Nevertheless, under certain circumstances such quartic terms can contribute in the same order as gradient squared terms, and it is convenient to retain the general form (2.2). Equivalently, we may write

$$\frac{\partial \psi}{\partial t} = \frac{1}{\tau_0}[\epsilon - \tilde{\xi}_0^4(\nabla^2 + q_0^2)^2 - g\psi^2]\,\psi. \tag{2.5}$$

Corrections to (2.5) are of relative order $\epsilon^{\frac{1}{2}}$ (Joseph 1976; Cross *et al.* 1980).

We shall now apply (2.5) to study various different geometrical configurations, and make explicit contact with the work of Newell & Whitehead (1969).

(i) *An infinite system of rolls parallel to the x direction:* We write

$$\psi(\mathbf{r}, t) = \sqrt{2}\,\mathrm{Re}\,[A(\mathbf{r}, t)\, e^{iq_0 x}], \tag{2.6}$$

where $A(\mathbf{r}, t)$ is a *complex* function. Equation (2.5) then becomes

$$\frac{\partial A}{\partial t} = \frac{1}{\tau_0}\left[\epsilon + \xi_0^2\left(\frac{\partial}{\partial x} - \frac{i}{2q_0}\frac{\partial^2}{\partial y^2}\right)^2 - g\,|A|^2\right] A(x, y, t), \tag{2.7}$$

with

$$\xi_0^2 = 4q_0^2\tilde{\xi}_0^4. \tag{2.8}$$

An analysis of the stability properties of steady solutions of (2.7) was carried out by Newell & Whitehead, who found the various stability boundaries appropriate to the limit $R \to R_c^\infty$, in agreement with results of Schlüter *et al* (1965) and Busse (1967*a*).

(ii) *An infinite system of N sets of rolls with orientations* $\hat{q}_i$ $(i = 1, \ldots, N)$: Let us set

$$\psi(\mathbf{r}, t) = \sqrt{2}\,\mathrm{Re}\left\{\sum_{i=1}^{N} A_i(\mathbf{r}, t)\, e^{i\mathbf{q}_i \cdot \mathbf{r}}\right\}, \tag{2.9}$$

with

$$|\mathbf{q}_i| = q_0. \tag{2.10}$$

Then the amplitude equation reads

$$\frac{\partial A_j}{\partial t} = \frac{1}{\tau_0}\left[\epsilon + \xi_0^2\left(\frac{\partial}{\partial x_j} - \frac{i}{2q_0}\frac{\partial^2}{\partial y_j^2}\right)^2 - \sum_l g_{jl}|A_l|^2\right]A_j, \tag{2.11}$$

where x_j is along $\mathbf{q}_j$. The coefficients g_{jl} depend on the angle $\hat{q}_j.\hat{q}_l$ and are Prandtl-number dependent (Newell & Whitehead 1969; Cross 1980), as discussed in appendix A.

(iii) *Concentric rolls in a cylinder.* For this case we write (Brown & Stewartson 1978)

$$\psi(\mathbf{r}, t) = \sqrt{2}\,\mathrm{Re}\,[(L/r)^{\frac{1}{2}} A(r, \theta, t)\, e^{iq_0 r}], \tag{2.12}$$

where r and θ are polar co-ordinates of $\mathbf{r}$ in the plane, and L is an arbitrary length scale which will be set equal to the cylinder radius below. The amplitude equation is then

$$\frac{\partial A}{\partial t} = \frac{1}{\tau_0}\left[\epsilon + \xi_0^2\left(\frac{\partial}{\partial r} - \frac{i}{2q_0 r^2}\frac{\partial^2}{\partial \theta^2}\right)^2 - \frac{gL}{r}|A|^2\right]A(r, \theta, t). \tag{2.13}$$

2.2. *Laterally finite system: boundary conditions*

The boundary conditions satisfied by ψ at lateral walls have only been derived for systems with free upper and lower boundaries. Moreover, since the amplitude equation allows only slow variations of ψ, it is clear that the lateral dimension of the container must be much larger than the height d. In that case, it has been shown (Brown & Stewartson 1977) that for a rectangular container (case (i) above), the boundary conditions at 'ideal' surfaces (either perfectly insulating or perfectly conducting) are

$$A(x, y) = 0 \quad \text{on} \quad x = \pm L, \tag{2.14a}$$

$$A(x, y) = \frac{\partial A}{\partial y} = 0 \quad \text{on} \quad y = \pm M, \tag{2.14b}$$

where $2L$ and $2M$ are the dimensions of the container perpendicular and parallel to the rolls, respectively. In fact, it may be shown (Cross *et al.* 1980) that (2.14*a*), in the direction perpendicular to the rolls, holds for rigid side walls of arbitrary thermal conductivity, as long as there is no heat loss through the walls in the static conduction state. In the opposite case where a heat current is imposed at the side walls,† the boundary condition (2.14*a*) takes the form (Daniels 1977)

$$A(x, y) = \lambda_\pm \quad \text{on} \quad x = \pm L, \tag{2.15}$$

where $\lambda_\pm$ depends on the heat current and the length L. The boundary condition (2.14*a*) has been dramatically confirmed in experiments by Wesfreid *et al.* (1978).

For a cylindrical container with cylindrically symmetric solutions, the boundary condition at the outside wall is the same as for a rectangular container, namely (2.14*a*) and (2.15) with x replaced by r. There is, however, an additional boundary condition at the centre of the cylinder, where the situation is somewhat complicated. Brown & Stewartson (1978) have shown that for sufficiently large radius L one may use the condition

$$A(r, \theta) = 0, \quad r = 0, \tag{2.16}$$

† This situation is somewhat misleadingly referred to as 'imperfectly insulating' in the recent literature.

whereas for finite but large L one has

$$A(0,\theta) = O(1/\ln L)^{\frac{1}{2}}, \tag{2.17}$$

so that the large L limit is only reached very slowly. We shall consider amplitude functions which vanish at the centre, as well as functions which are finite. The boundary conditions for non-cylindrically-symmetric solutions have not been discussed, as far as we know, in cylindrical geometry.

2.3. *Removal of spatial dependence*

The partial differential equation (2.5) can be reduced to an ordinary differential equation in time, under two different sets of conditions. The first is the case of a very large system, not too near the threshold, when the spatial dependence of the solution may be neglected, namely

$$\epsilon(L/\pi\xi_0)^2 \gg 1, \tag{2.18}$$

with nevertheless $\epsilon \ll 1$. For the rectangular system the appropriate equation is obtained from (2.7) by neglecting the spatial dependence of $A(r,t)$,

$$\frac{dA(t)}{dt} = \frac{1}{\tau_0}[\epsilon - g|A|^2]A(t). \tag{2.19}$$

For the cylinder the same equation holds, applicable in the region $1 \ll r < L$, where the derivative term in (2.13) is negligible.

The other limit in which the spatial structure of A may be neglected is near the threshold, where only the lowest unstable mode of the linear system is excited. Let us, for illustration, consider the cylindrically symmetric case, namely (2.13) with no θ dependence

$$\frac{\partial A}{\partial t} = \frac{1}{\tau_0}\left[\epsilon + \xi_0^2\frac{\partial^2}{\partial r^2} - \frac{gL}{r}|A|^2\right]A(r,t), \tag{2.20}$$

and boundary conditions

$$A(r = L,t) = A(r = 0,t) = 0. \tag{2.21}$$

We expand the solution in the form

$$A(r,t) = \sum_{n=1}^{\infty} A_n \sin\frac{n\pi r}{L}, \tag{2.22}$$

and derive coupled equations for the A_n. As shown in appendix B, a closed equation for the largest amplitude $A_1 \equiv \bar{A}$ results, in the range

$$\epsilon(L/\pi\xi_0)^2 \approx 1. \tag{2.23}$$

This equation has the form

$$\frac{d\bar{A}}{dt} = \frac{1}{\bar{\tau}_0}[\bar{\epsilon} - \bar{g}|\bar{A}|^2]\bar{A}, \tag{2.24}$$

where

$$\bar{\epsilon} = \frac{\epsilon - \epsilon_c}{1+\epsilon_c} = \frac{R - R_c}{R_c}, \quad \epsilon_c \equiv \pi^2\xi_0^2/L^2 = \frac{R_c - R_c^\infty}{R_c^\infty}, \tag{2.25), (2.26}$$

$$\bar{g} = 1{\cdot}6595g(1+\epsilon_c)^{-1}, \quad \bar{\tau}_0 = \tau_0(1+\epsilon_c)^{-1}. \tag{2.27), (2.28}$$

The domain of validity of (2.24) is more properly written as

$$\bar{\epsilon} \lesssim \epsilon_c, \tag{2.29}$$

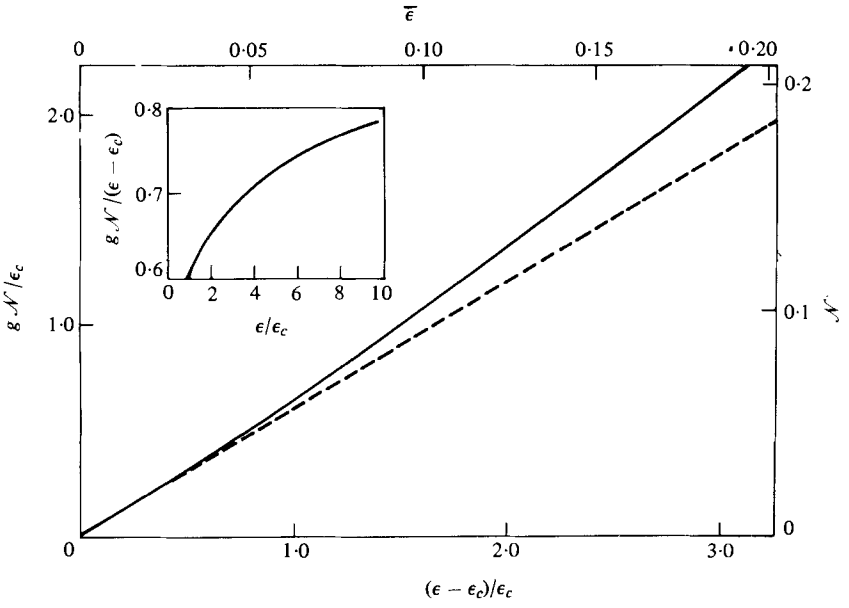

FIGURE 1. Convective heat flow $\mathcal{N}$ from the static solution of the amplitude equation for a cylinder [equation (2.20), solid line] as a function of reduced Rayleigh number $\epsilon = (R - R_c^\infty)/R_c^\infty$. The plot of $g\mathcal{N}/\epsilon_c$ *vs.* $(\epsilon - \epsilon_c)/\epsilon_c$ (where $\epsilon_c \equiv \pi^2\xi_0^2/L^2$) is independent of the cylinder radius L. The upper and right-hand scales ($\mathcal{N}$ *vs.* $\bar{\epsilon}$) depend on L and σ and are evaluated for the experimental values $L = 4{\cdot}72$ ($\epsilon_c = 0{\cdot}066$) and $\sigma = 0{\cdot}78$. The dashed line is the single-mode approximation, equation (2·24). The inset shows the 'slope' of the solid curve. Note that the slope appropriate to the infinite system [$g\mathcal{N}/(\epsilon - \epsilon_c) = 1$] is not reached until $\epsilon/\epsilon_c \gg 1$.

i.e. the ordinary differential equation is only strictly valid in the immediate vicinity of the (shifted) threshold. As $\bar{\epsilon}$ increases, the higher modes of (2.22) are coupled in, and one must solve a partial differential equation in order to describe the region intermediate between (2.18) and (2.29). We would in principle expect corrections to (2.24)–(2.28) to be of order $\epsilon_c^{\frac{1}{2}}$, which is 0·24 for the value $L = 4{\cdot}72$ used in our experiments. On the other hand, comparison with exact calculations of the growth rate $\bar{\tau}_0$ using the linear theory in finite geometry (Shaumeyer, Behringer & Baierlein 1980, and private communication) suggest that the accuracy is higher, possibly of order ϵ_c. Indeed, for $L = 4{\cdot}72$ and $\sigma = 0{\cdot}78$, these authors find $\bar{\tau}_0^{-1} = 12{\cdot}25$ for conducting lateral boundaries, and $\bar{\tau}_0^{-1} = 12{\cdot}48$ for insulating boundaries, in excellent agreement with the value $\bar{\tau}_0^{-1} = 12{\cdot}58$ obtained from (2.28), which does not differentiate between conducting and insulating boundaries to lowest order.

As an example of the existence of the different regimes (2.18) and (2.29), we have calculated the static solutions of the partial differential equation (2.20) for cylindrical geometry. The ensuing heat flow is plotted in figure 1, as a function of ϵ, along with the single-mode approximation (2.24). It is seen from the figure that the crossover to the large system behaviour described by (2.19) is rather slow.

Experimental measurements of static Nusselt numbers for $0 < \bar{\epsilon} < 0{\cdot}08$ in cell A with $L = 4{\cdot}72$, closely agree with the expression (Behringer & Ahlers 1982)

$$\mathcal{N}_{\rm st} = 0{\cdot}840\bar{\epsilon} + 0{\cdot}64\bar{\epsilon}^2. \tag{2.30}$$

A fit to the solid curve in figure 1 gives a coefficient of $\bar{\epsilon}$ that is 7 % larger. The coefficient

of $\bar{\epsilon}^2$ differs by 30 %, but it is not well characterized by either experiment or theory, since it depends sensitively on the linear coefficient, and the range of the fit. Notice that contrary to the suggestion of Behringer & Ahlers (1977) the initial slope $\mathcal{N}/(\epsilon-\epsilon_c)$ is predicted to be independent of aspect ratio (and equal to $0{\cdot}60g^{-1}$) *provided* it is measured sufficiently close to onset, i.e. for $\bar{\epsilon} \ll \epsilon_c$. In large systems, only measurements at very small $\bar{\epsilon}$ will give this initial slope.

2.4. *Forcing term: effect of imperfections and fluctuations*

The preceding discussion of the amplitude equation with boundary conditions represents an exact rewriting of the hydrodynamic equations, for the case of slow variations in space and time, with R near R_c. We wish to apply the equation to a situation in which the temperature of the bottom plate is time dependent, which implies that the Rayleigh number R will vary in time. It is clear, however, that if the effect of external heating is modelled solely by a time-dependent R, then the amplitude equation (2.5), being *homogeneous* in ψ, will never show a transition from a non-convecting state ($\psi = 0$) to a convecting one ($\psi \neq 0$). In order to treat this transition we will depart from the point of view based on a strict expansion of the hydrodynamic equations, and introduce a *phenomenological* term in the amplitude equation, modifying (2.5) to read

$$\frac{\partial \psi}{\partial t} = \frac{1}{\tau_0}[\epsilon - \tilde{\xi}_0^4(\nabla^2 + q_0^2)^2 - g\psi^2]\psi(\mathbf{r},t) + f(\mathbf{r},t). \tag{2.31}$$

The form of f is not known *a priori*, and we shall use it as a phenomenological parameter to fit the measurements on the response of the system to time-dependent heating. A number of physical mechanisms may be identified, which can be modelled at least approximately by such an inhomogeneous term. The simplest, perhaps, is a static imperfection in the cell geometry, which prevents the system from undergoing a true bifurcation in its time-independent solution (Kelly & Pal 1976; Daniels 1977; Hall & Walton 1977). The 'imperfect' boundary condition (2.15) is an example of such an effect. Another mechanism which can produce a forcing term in (2.31) is the lateral heat flow induced by the time dependence of the heating (see appendix C). In general, we may cite the effect of the fast hydrodynamic modes which have been projected out in deriving the homogeneous equation (see appendix A). When the system is heated at a finite rate it is expected that these modes will couple to the order parameter ψ in some complicated way, which we shall model via f. Finally, fluctuation effects can be included approximately in (2.31), either by choosing random initial conditions (Newell, Lange & Aucoin 1970) or if we consider f to be a stochastic variable with a specified probability distribution. The most basic such effect is the Langevin force arising from molecular thermal fluctuations, which can be represented by a Gaussian white noise source with correlations

$$\langle f(\mathbf{r},t) f(\mathbf{r}',t')\rangle = \frac{2}{\tau_0} F\,\delta(t-t')\,\delta(\mathbf{r}-\mathbf{r}'), \tag{2.32}$$

(Zaitsev & Shliomis 1970; Graham 1974; Swift & Hohenberg 1977). The magnitude of F for thermal noise is obtained in appendix D for the case of free–free boundary conditions. Its value is

$$F_{\mathrm{th}} = \left(\frac{k_B T}{\nu^2 \rho d}\right)\left(\frac{\sigma^2}{1+\sigma}\right)\left(\frac{3}{R_c}\right)^{\frac{1}{2}}. \tag{2.33}$$

Inserting typical experimental values for *He* at low temperatures, we obtain the value

$$F_{\text{th}} = 3{\cdot}6 \times 10^{-9}, \tag{2.34}$$

which is of course very small, since it represents the effect of molecular noise on a macroscopic phenomenon. The above estimate is based on a calculation of thermal fluctuations in equilibrium, assuming that the macroscopic motion in the cell does not react back on the molecular noise. It is conceivable, however, that nonlinear interactions among the hydrodynamic modes could serve to enhance the thermal noise compared with its equilibrium value, although this appears to us unlikely to occur near R_c. With this possibility in mind, however, and also with the aim of modelling extrinsic sources of noise coming from the apparatus, we shall analyse a stochastic system given by (2.31) and (2.32), with F treated as an adjustable parameter.

It should be noted that the necessity for a deviation from the conducting state before the convecting solution can grow, is not connected with the gradient expansion used to obtain (2.5). Indeed, the full Boussinesq equations [equations (A 1)–(A 4) of appendix A] also require nonzero initial disturbances in order to describe the convective onset (Davis 1971). The quantity f in (2.31) is merely a convenient parametrization of this initial disturbance, insofar as it affects the growth of the convective pattern. Since this growth is slow [with a rate of $O(\epsilon)$], the amplitude equation provides an exact description of the process after the fast transients have decayed to zero.

3. Time-dependent heating experiments

The apparatus and experimental procedures used for this work are described in detail in a separate paper by Behringer & Ahlers (1982). The fluid was normal (i.e. non-superfluid) liquid ^{4}He at a temperature of 2·1841 K at saturated vapour pressure. It had a Prandtl number $\sigma = 0{\cdot}78$. Near the Rayleigh–Bénard threshold, the system can be described well by the Boussinesq equations, with departures from this approximation yielding a value of 0·2 for the parameter P defined by Busse (1967*b*) (see also Ahlers 1980).

Measurements were made primarily in cell A, with $L = 4{\cdot}72$, and to a lesser extent in cell B with $L = 2{\cdot}08$. The experiments were conducted by applying a computer-generated, time-dependent voltage to a heater at the bottom of the cell while holding the temperature T_u at the top of the cell at a constant value. The resulting heat current $\bar{Q}(t)$ (see equation (C 7) for the normalization of $\bar{Q}$) produced a time-dependent temperature response of the system, and the temperature $T_l(t)$ at the bottom was measured at fixed time intervals by the computer and associated electronic circuitry (Behringer & Ahlers 1982).

Throughout an experimental run, $T_l(t)$ was measured at fixed dimensionless time intervals about equal to 0·1. Typically such a run consisted of the following sequence of events:

(i) $\bar{Q}$ was set to zero for a period of about 1 h (dimensionless time interval $\delta t \approx 12$) to establish the absence of all transients and a baseline for the measurement of T_l.

(ii) The heat current was discontinuously changed to $\bar{Q} = \bar{Q}_0 < \bar{Q}_c$, where $\bar{Q}_c$ is the value of $\bar{Q}$ needed to produce $R = R_c$ in the steady state. This condition was maintained for one to three hours, depending on the size of $\bar{Q}_c - \bar{Q}_0$. For small values, long equili-

bration times were considered necessary to permit the system to reach a steady state under the influence of a forcing term like $f(\mathbf{r},t)$ in (2.31).

(iii) $\bar{Q}$ was changed from $\bar{Q}_0$ to $\bar{Q}_1 > \bar{Q}_c$, either in a step or by means of a linear ramp. Explicitly, for the step,

$$\bar{Q}(t) = \bar{Q}_0 \quad \text{for} \quad t < t_0 < 0, \tag{3.1a}$$

and

$$\bar{Q}(t) = \bar{Q}_1 \quad \text{for} \quad t > t_0. \tag{3.1b}$$

For the ramp,

$$\bar{Q}(t) = \bar{Q}_0 \quad \text{for} \quad t < t_0 < 0, \tag{3.2a}$$

and

$$\bar{Q}(t) = \bar{Q}_0 + \gamma(t - t_0) \quad \text{for} \quad t > t_0, \tag{3.2b}$$

where $\gamma = d\bar{Q}/dt$ is the ramp rate. For the step or the ramp, the time origin is chosen when $\bar{\epsilon} = 0$.

(iv) Whenever possible, $\bar{Q}_1$ was maintained for a time period sufficient to establish a steady state. When $\bar{Q}_1$ was too large, a time-independent state of the system did not exist (Ahlers & Walden 1980), and this segment of the run was terminated after one or two hours. (An example is shown in figure 8 below.)

(v) $\bar{Q}$ was changed back to $\bar{Q}_0$ to establish the overall stability of the apparatus for the duration of the run.

(vi) $\bar{Q}$ was changed to zero as a further stability check.

The overall accuracy of the measurements was limited primarily by variations in $\bar{Q}$ due to variations of order 10^{-9} W in the background heat input to the system (Behringer & Ahlers 1982), and for cell A was slightly better than 0·001 in $\mathcal{N}$ or $\bar{Q}$. For cell B, the stability was not as high because the smaller cross-sectional area resulted in a larger response to variations in $\bar{Q}$. For that reason, cell B was used primarily for the determination of t_{on} *vs.* γ, and detailed studies of $\mathcal{N}(t)$ were confined to cell A ($L = 4{\cdot}72$). All data in figures 2–8 and 11–16 are for cell A.

4. Analysis of experiments

4.1. *Basic equations*

Since the externally controlled quantity in the experiments is the heat current Q, rather than the Rayleigh number, it is necessary first to relate the time dependences of these two quantities even in the absence of convection. In appendix C it is shown that this relation is

$$Q(t) \equiv \bar{Q}(t) - \bar{Q}_c = (1 + \lambda_w)\,\bar{\epsilon}(t) + c_1 \frac{d\bar{\epsilon}}{dt}, \tag{4.1}$$

where λ_w is the contribution to conductance coming from the side walls, and c_1 is a parameter of order unity. In the presence of convection there is an additional heat current, which in dimensionless form is just $\mathcal{N}$, so that using (2.4), (4.1) becomes

$$Q(t) = (1 + \lambda_w)\,\bar{\epsilon}(t) + c_1 \frac{d\bar{\epsilon}}{dt} + \frac{1}{S}\int d^2r\, \psi^2(\mathbf{r},t). \tag{4.2}$$

The above equation must be solved in conjunction with the time-dependent amplitude equation (2.31) for given $Q(t)$, to obtain $\psi(\mathbf{r},t)$ and $\bar{\epsilon}(t)$, and then the convection heat current $\mathcal{N}$, via (2.4).

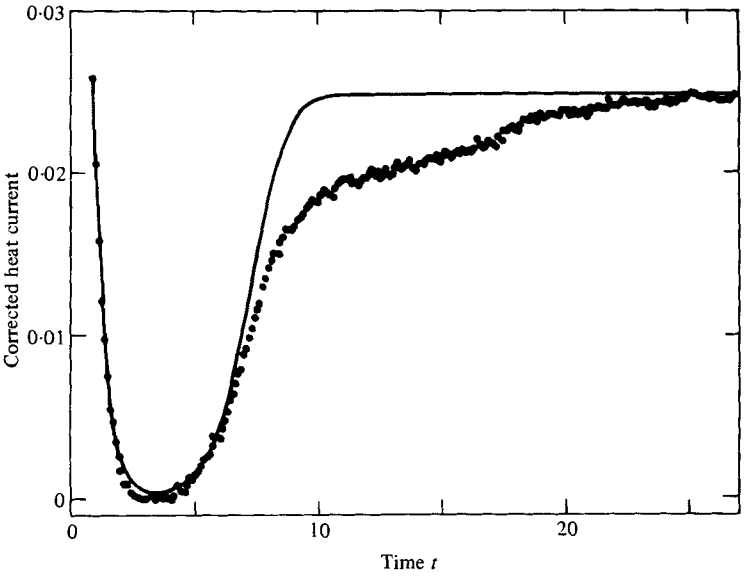

FIGURE 2. Corrected heat current as a function of time (in units of d^2/κ) for a step in the heat input at $t_0 = 0$, with the parameter values $\bar{\epsilon}_0 = 0{\cdot}14$ and $\bar{\epsilon}_1 = 0{\cdot}049$ in equations (4.7) and (4.8). As explained in appendix C, the corrected heat current is essentially equal to the convective heat current $\mathcal{N}$ for $t > 3$, but differs from zero for $t < 3$, before convection sets in, due to the finite response time of the conducting solution. The solid line is a fit to the deterministic one-mode equation for rolls, equations (4.3)–(4.6), with the field strength $\bar{f}$ adjusted.

4.2. *Analysis in terms of a single roll pattern*

Let us assume that the pattern which grows initially is the lowest state, $n = 1$, of some set of modes satisfying the boundary condition (2.14). For the moment we shall not specify the particular symmetry of the structure. The amplitude of the mode satisfies an equation depending only on time, which is written, according to (2.24), as

$$\frac{d\bar{A}}{dt} = \frac{1}{\bar{\tau}_0}[\bar{\epsilon}(t) - \bar{g}\,|\bar{A}|^2]\bar{A} + \bar{f}, \tag{4.3}$$

where the value of $\bar{g}$ depends on the precise form of the mode excited. In the present analysis we shall first use the $\bar{g}$ obtained from independent static measurements of the slope of the Nusselt number as a function of Rayleigh number (Behringer & Ahlers 1982)

$$\mathcal{N}_{st} = \mathcal{N}(\bar{\epsilon}) = \bar{\epsilon}/\bar{g}_{\exp}. \tag{4.4}$$

In the time-dependent situation $\bar{\epsilon}(t)$ is given in terms of the externally imposed $Q(t)$ by

$$(1 + \lambda_w)\,\bar{\epsilon} + c_1 \frac{d\bar{\epsilon}}{dt} = [Q(t) - \mathcal{N}(t)] \tag{4.5}$$

with

$$\mathcal{N}(t) = |\bar{A}|^2. \tag{4.6}$$

We have solved (4.3) and (4.5) numerically for both the jump and the ramp in $Q(t)$, and have fitted the ensuing $\mathcal{N}(t)$ to the experimental data, using the constant $\bar{f}$ as an adjustable parameter. It may be seen from the form of (4.3) that $\bar{f}$ determines primarily

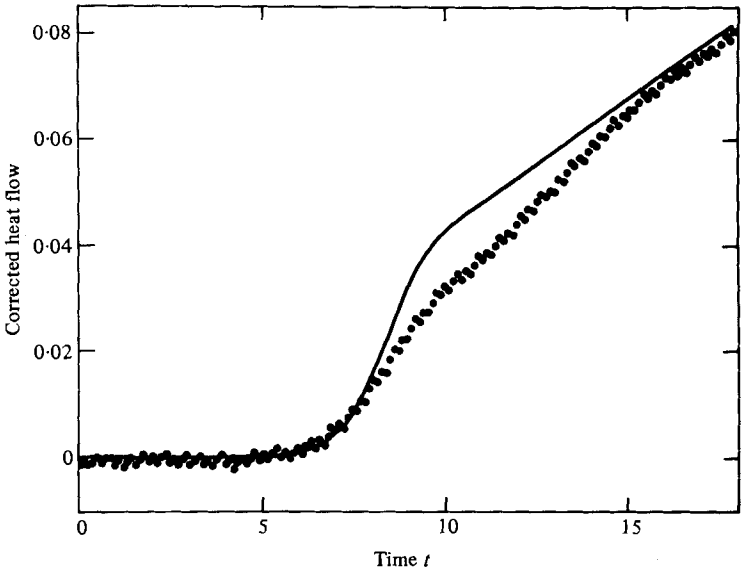

FIGURE 3. The same plot as in figure 2, for a ramp in the heat input, corresponding to the parameter values $\bar{\epsilon}_0 = 0{\cdot}051$, and $t_0 = \bar{\epsilon}_0/\beta$ in equations (4.9) and (4.10). $\beta = 0{\cdot}01$.

the onset time for convection, whereas the magnitude of $\mathcal{N}$ at later times is fixed primarily by $\bar{g}$, obtained from (4.4).

Figure 2 shows the measured values of the heat flow in a step experiment [see (3.1)]. In practice, as explained in appendix C, it is more convenient to consider a 'corrected heat flow' both experimentally and theoretically, but the correction is only large at early times, before convection sets in. Moreover, the different runs are characterized by the reduced Rayleigh numbers $\bar{\epsilon}(t)$ rather than the heat input $Q(t)$ of (3.1)–(3.2). Thus the step experiment has

$$\bar{\epsilon}(t) = -\bar{\epsilon}_0, \quad t < t_0, \tag{4.7}$$

and

$$\bar{\epsilon}(t) = \bar{\epsilon}_1, \quad t > t_0, \tag{4.8}$$

where (4.8) refers to times such that initial transients have died, but convection has not yet set in. The solid line in figure 2 is the fit to (4.4)–(4.6) for a simple roll pattern, with the value of the field $\bar{f}$ adjusted. Figure 3 shows the analogous information for a ramp in $Q(t)$ [equation (3.2)], which we parametrize in terms of $\bar{\epsilon}$ as

$$\bar{\epsilon}(t) = -\bar{\epsilon}_0, \quad t < t_0, \tag{4.9}$$

and

$$\bar{\epsilon}(t) = -\bar{\epsilon}_0 + \beta(t - t_0), \quad t > t_0, \tag{4.10}$$

where (4.10) again refers to times such that initial transients have died but convection has not set in. As shown in (C 12) the ramp rate β is related to the ramp in $Q(t)$ (equation (3.2*b*)] by $\beta = \gamma(1 + \lambda_w)^{-1}$. It is clear from figures 2 and 3 that the theory does not account quantitatively for the experimental time dependence of $\mathcal{N}$. In particular, it appears that, instead of going directly to its final state, the system first enters an intermediate state, with a lower value of $\mathcal{N}$. It may be noted, moreover, that the ratio of this value of $\mathcal{N}$ to the stable value is equal to the ratio of static $\mathcal{N}$ values for hexagons

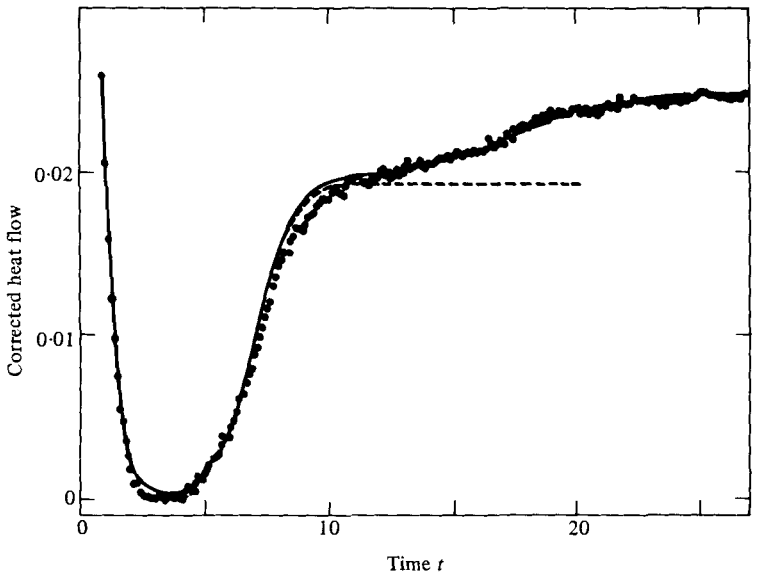

FIGURE 4. The data of figure 2 are plotted, along with a fit to the deterministic equation for hexagons and rolls [equation (4.11)], with two field parameters $\bar{f}_1$ and $\bar{f}_2$ adjusted. The dashed line is the pure hexagon solution ($\bar{f}_1 = \bar{f}_2$).

and rolls in an infinite system. We have therefore attempted to fit the data by assuming that the intermediate state represents a hexagonal pattern,† as described in the next section.

4.3. *Analysis in terms of hexagons and rolls*

In order to approximate the hexagon pattern we shall assume that the initial disturbance consists of three sets of rolls, each one analogous to the set considered in the previous section. The different sets are oriented at an angle of $\frac{2}{3}\pi$ with respect to one another. Then, according to the analysis of appendix B, there are coupled amplitude equations of the form

$$\frac{d\bar{A}_i}{dt} = \frac{1}{\bar{\tau}_0}\left\{\bar{\epsilon}(t) - \bar{g}\left[\sum_j |\bar{A}_j|^2 + \bar{\beta}\sum_{j\neq i}|\bar{A}_j|^2\right]\right\}\bar{A}_i + \bar{f}_i, \quad i = 1,2,3, \tag{4.11}$$

with

$$\mathcal{N}(t) = \sum_{i=1}^{3}|\bar{A}_i|^2. \tag{4.12}$$

The relation determining $\bar{\epsilon}(t)$ in terms of Q is still (4.5). It may be noted that, if the $\bar{f}_i$ are all equal, the final state will be a hexagonal pattern with $\bar{A}_1 = \bar{A}_2 = \bar{A}_3 = \bar{A}$ and a static Nusselt number

$$\mathcal{N}_{\text{hex}} = \left[\bar{g}\left(1+\frac{2\bar{\beta}}{3}\right)\right]^{-1}\bar{\epsilon}. \tag{4.13}$$

On the other hand, if $\bar{f}_1 > \bar{f}_2, \bar{f}_3$ then $\bar{A}_2$ and $\bar{A}_3$ eventually decay to zero and we have

$$\mathcal{N}_{\text{roll}} = (\bar{g})^{-1}\bar{\epsilon}, \tag{4.14}$$

as in (4.4). In order to fit the data in figures 2 and 3 we have used the theoretical value

† We are indebted to Robert Graham for this remark.

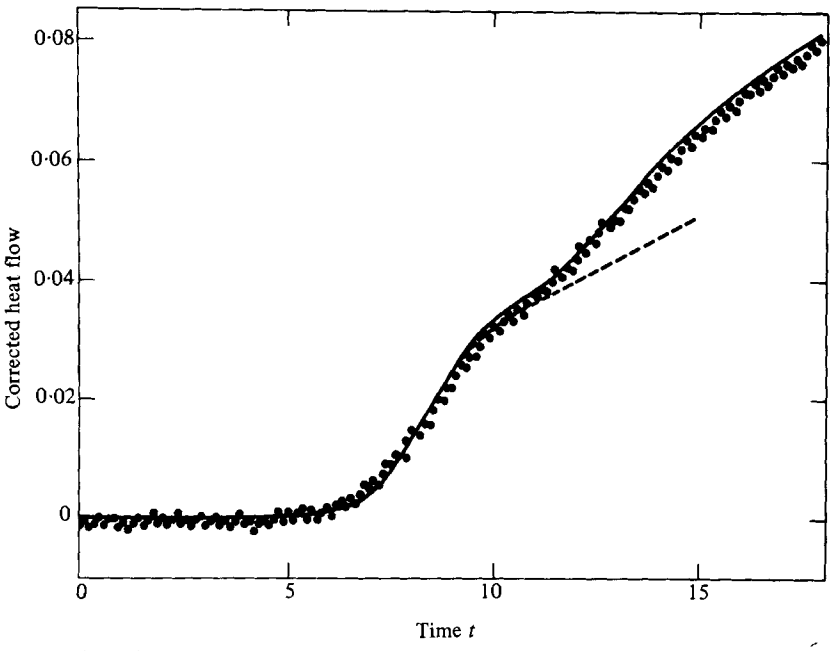

FIGURE 5. The data of figure 3 are plotted, along with a fit to equation (4.11), for hexagons and rolls. The dashed line is the pure hexagon solution. $\beta = 0{\cdot}01$.

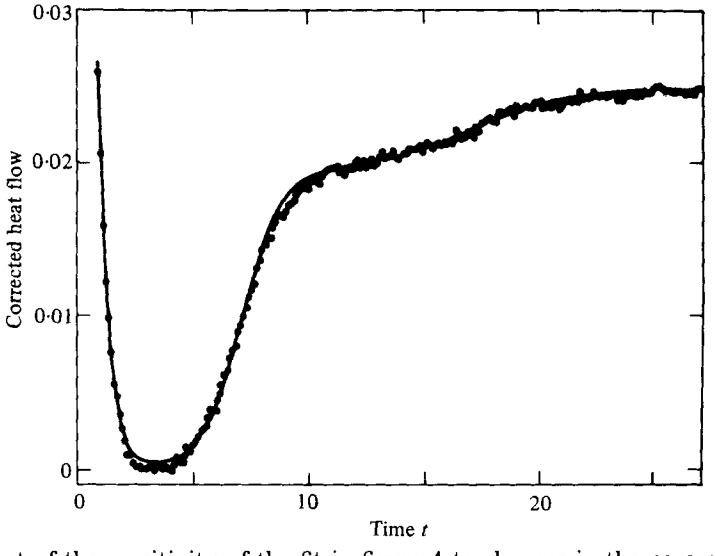

FIGURE 6. Test of the sensitivity of the fit in figure 4 to changes in the parameters. The time scale $\bar{\tau}_0$ has been increased by 7% and the hexagon coefficient $\bar{\beta}$ of equation (4.11) has been increased by 6%.

($\bar{\beta} = 0{\cdot}77$) from table 1. We have chosen $\bar{f}_2 = \bar{f}_3 < \bar{f}_1$, and have adjusted the *two* parameters $\bar{f}_1$ and $\bar{f}_2$. The results are presented in figures 4 and 5, and show a marked improvement over the previous fits. In particular, the value of $\mathcal{N}$ in the intermediate state is determined by the parameter $\bar{\beta}$ of (4.11), which follows from the assumption of hexagons, rather than from the fit. Thus the agreement between experiment and theory in the time intervals $10 \lesssim t \lesssim 20$ in figure 4 and $10 \lesssim t \lesssim 15$ in figure 5 may be

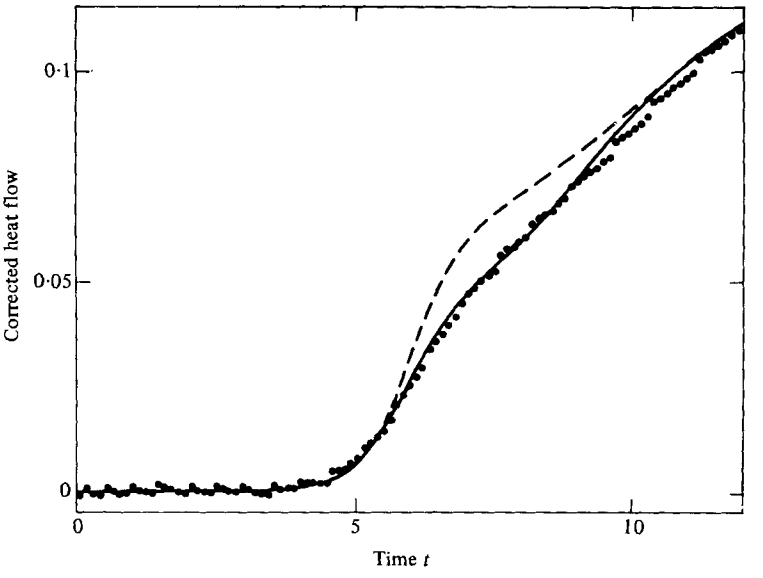

FIGURE 7. The same plot as in figure 3 for a higher ramp rate, $\beta = 0{\cdot}02$. The dashed line is the pure roll solution ($\bar{f}_2 = 0$).

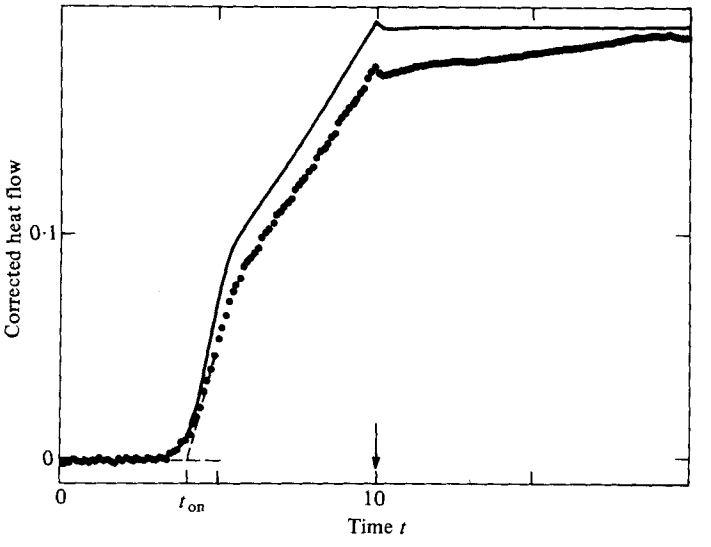

FIGURE 8. The same plot as in figure 3, for a higher ramp rate, $\beta = 0{\cdot}037$. The arrow at $t = 10$ denotes the time at which the ramp was shut off. The onset time t_{on} is obtained by a linear extrapolation of the data to zero heat flow.

considered evidence in favour of the hexagons. Note, however, that the values of $\bar{f}_1$ and $\bar{f}_2$ are chosen independently for the jump and the ramp.

Further improvements of the fits can be obtained by small shifts in the other parameters $\bar{\tau}_0$, $\bar{\beta}$, and $\bar{g}$. For the step data an increase in $\bar{\tau}_0$ by 7 % and in increase in $\bar{\beta}$, by 6 %, yield a fit which is within the scatter of the data, as shown for example in figure 6. In addition, there is enough scatter in the static measurements leading to (4.4) at small

$\bar{\epsilon}$, that $\bar{g}$ must be adjusted by about 5 % from run to run in the step experiments, in order to fit the data at long times. (The scatter in the static data is evident in figure 14 below.)

We may attempt to infer the form of the final roll pattern from the measured slope of $\mathcal{N}$ *vs.* $\bar{\epsilon}$ in steady state, i.e. from the experimental value, $\bar{g}_{\text{exp}} = 1{\cdot}19$, in (4.4). The theoretical estimates in appendix B are $\bar{g} = 1{\cdot}10$ for concentric rolls with a node at the centre, $\bar{g} = 1{\cdot}38$ for straight rolls, and $\bar{g} = 2{\cdot}2$ for concentric rolls with finite amplitude at the centre. A comparison of the slopes favours concentric rolls with a node at the centre, and the analysis of §2.3 was done for this pattern. Other evidence, however, (Stork & Müller 1975; Behringer & Ahlers 1982) suggests a pattern of straight rolls for which the estimated slope is in slightly worse agreement with experiment. The analysis of §§4.2 and 4.3 depends on the symmetry of the basic roll pattern primarily through the parameter $\bar{g}$, which was taken from experiment. Additional small corrections due to different threshold values ϵ_c for different patterns do not significantly affect the predicted temporal evolution.

Comparable fits to the ones shown in figure 4 are obtained for other step values in the range $0{\cdot}04 < \bar{\epsilon}_0 < 0{\cdot}2$ and $0{\cdot}04 < \bar{\epsilon}_1 < 0{\cdot}07$. Ramp experiments with a number of different ramp rates were also carried out, as shown in figures 7 and 8. Since rather large $\bar{\epsilon}$ are included in these runs it is necessary to include the next-order terms in the amplitude equation as displayed in (B 7) in appendix B. Again the coefficient $\bar{g}_6$ is taken from the static experiments as given by (2.30). For the ramp rate $\beta = 0{\cdot}037$ in figure 8, and higher ones not shown, the theory based on unstable hexagons followed by stable rolls did not fit the data beyond the onset of convection. In those cases the system reached a value of $\mathcal{N}$ which was outside the range of validity of the amplitude equation before any convective pattern was established, and it is much more difficult to do a quantitative theory. In figure 8 for example, we may note the slow drift of the system up to its steady-state value, after the ramp was turned off at $t \approx 10$. Such effects were also seen at the higher ramps, and appear to be related to the onset of turbulence, which becomes noticeable in steady state around $\mathcal{N} = 0{\cdot}3$ (Ahlers & Walden 1980). The systematics of the onset time as a function of ramp rate, will be discussed further in §4.6 below.

4.4. *The partial differential equation*

It is of interest to consider the amplitude equation without making the single-mode approximation which eliminates all spatial diffusion effects. Indeed, it might be thought that the deviations from the fit to a roll pattern in figure 2 come from the appearance of another time scale, reflecting the diffusion of the initial disturbance from the periphery of the cell into the interior. Unfortunately, the full amplitude equation (2.13) in two space dimensions and one time dimension is too difficult to treat numerically, so we have restricted ourselves to the axially symmetric roll system (2.20). The equation determining $\epsilon(t)$ was approximated by dropping the $d\epsilon/dt$ term in (4.2), since this term has essentially no effect for $t > 3$. Instead of a forcing function f in (2.13), the process was started by using a boundary condition

$$A(r = L, t) = f_B \tag{4.15}$$

for all times, and f_B was adjusted to fit the data. The boundary condition at the centre was taken as (2.16). The partial differential equation was solved using a method

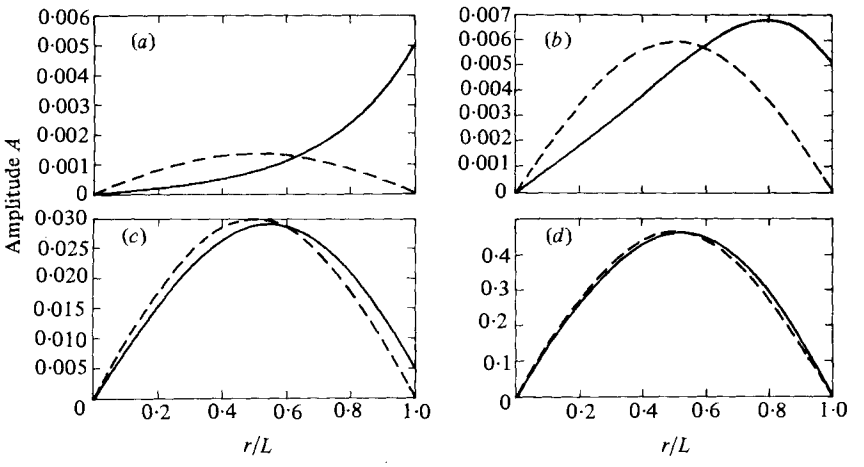

FIGURE 9. Results of numerical integration of the amplitude equation (2.20) for rolls, with fixed boundary values $A(r = 0) = 0$, $A(r = L) = f_B$, solid line (note the different vertical scales on the different curves). The dashed line is the one-mode approximation (4.3)–(4.6) whose heat flow is represented in figure 2. (*a*) $t = 0$; (*b*) $t = 1$; (*c*) $t = 3$; (*d*) $t = 10$.

developed by Schryer (1977), and the resulting heat current turned out to be indistinguishable from that of the single-mode calculation shown in figure 2. In particular the behaviour associated with the propagation of the disturbance into the bulk would not show up on the scale of the figure.

The time evolution of the amplitude is shown in figure 9 and compared with the amplitude

$$A(r,t) = \bar{A}(t)\sin\frac{\pi r}{L}, \tag{4.16}$$

obtained from the single-mode approximation. Since the boundary condition (4.15) for the partial differential equation is different from (2.21), the shape function differs from (4.16) near the edge at all times, but the difference becomes relatively less important as the overall amplitudes grow. We conclude from this comparison that the single-mode approximation to (2.20) works quite well at all times at which $\mathcal{N}$ differs visibly from zero, and the diffusion process cannot be invoked to explain the disagreement in figure 2 between the data and the theory with a single roll pattern.

4.5. *The stochastic equation*

As discussed in § 2(*d*), we have explored the possibility that the forcing term f might be stochastic in origin. Since the solution of a nonlinear stochastic equation is much more difficult than that of a deterministic equation, we have confined our analysis to the study of a single mode problem, such as (4.3), with a random external force. In order to make contact with experiment we have only considered the intermediate (hexagon) state which is excited initially, and have discarded the data involving the final (roll) state. We thus wish to fit the time dependence of the heat flow up to $t = 12$, say, in figures 2 and 3, using the stochastic model. Here again, the set of coupled equations (4.3)–(4.6) is too difficult to solve, so we have neglected the time derivative term in (4.5), which contributes primarily to the heat transport before the onset of

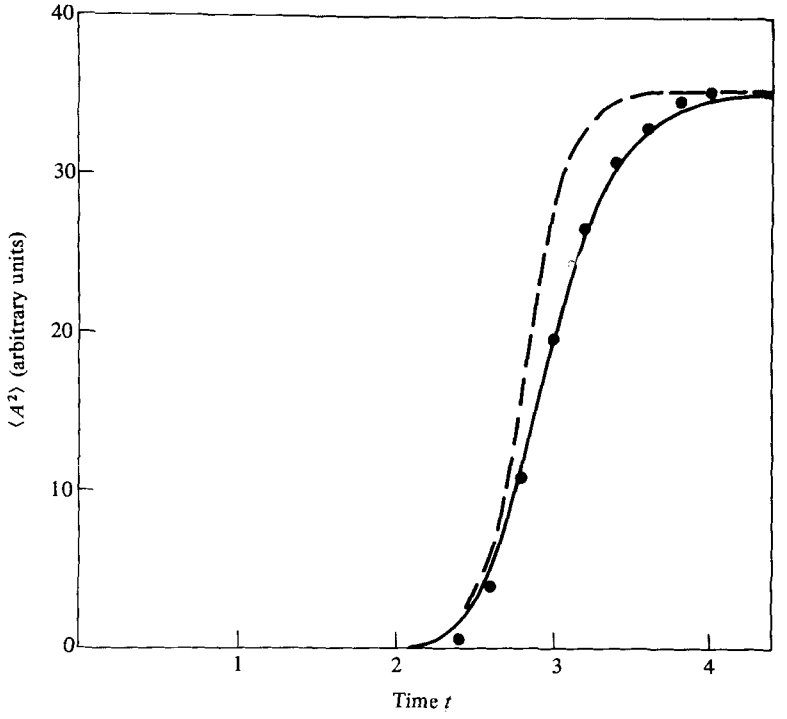

FIGURE 10. Integration of stochastic equation analogous to (4.17) for a step in $\epsilon(t)$ at $t = 0$. The dots are the numerical solution of Jhaveri & Homsy (1980), the solid line is the approximation (D 10), and the dashed line follows from the decoupling approximation (4.21).

convection ($t < 3$ in figure 2). Then the coupled set reduces to the single stochastic equation

$$\frac{d\bar{A}}{dt} = \frac{1}{\bar{\tau}_0}[Q(t) - \tilde{g}\,|\bar{A}|^2]\bar{A}(t) + \bar{f}(t), \tag{4.17}$$

with

$$\tilde{g} = \bar{g}\left(1 + \frac{2\bar{\beta}}{3}\right) + (1+\lambda_w)^{-1}, \tag{4.18}$$

$$\mathcal{N}(t) = \langle |\bar{A}|^2 \rangle, \tag{4.19}$$

and a white noise spectrum assumed for $\bar{f}(t)$,

$$\langle \bar{f}(t)\bar{f}(t') \rangle = 2\bar{\tau}_0^{-1}\bar{F}\,\delta(t-t'). \tag{4.20}$$

The relation between $\bar{F}$ and the parameter F of (2.32) is discussed in appendix D.

This nonlinear stochastic equation cannot be solved analytically, and a full numerical solution involves considerable computation. Instead, we have generalized a method originally due to Suzuki (1978) which yields an approximate analytic solution of the equation, as outlined in appendix D. The method interpolates between the linear stochastic equation ($\tilde{g} = 0$) at early times, and the nonlinear deterministic equation ($\bar{f} = 0$) at late times where the noise in negligible. Although this interpolation is carried out in an uncontrolled way, we have tested it for the simple case of a step function in $Q(t)$, against a numerical solution due to Jhaveri & Homsy (1980). The result is shown

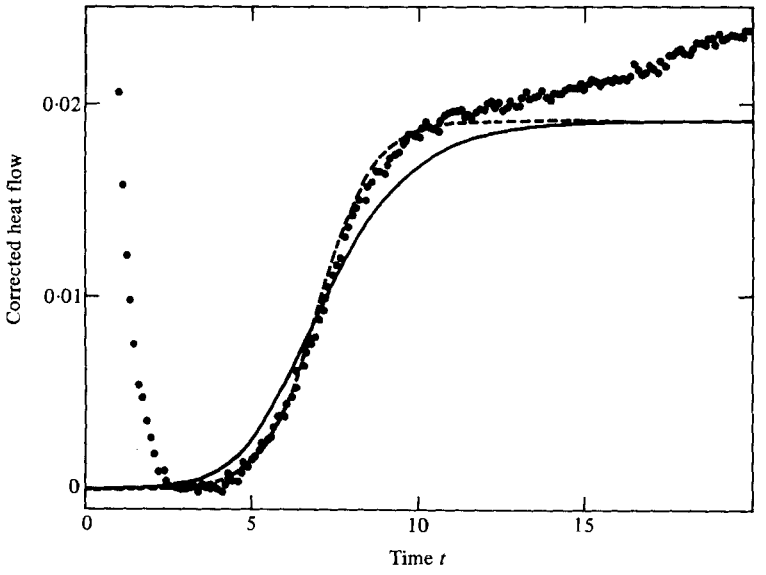

FIGURE 11. The same data as in figure 2, along with a fit to the stochastic equation (solid line) for hexagons only, with the noise strength $\bar{F}$ adjusted. The dashed line is the deterministic fit, analogous to the dashed line in figure 4. The transients for $t < 3$ are not included in the theoretical curves.

in figure 10, where it is also compared to a decoupling approximation, obtained by setting

$$\langle |A|^4 \rangle = [\langle |A|^2 \rangle]^2, \tag{4.21}$$

and solving the ensuing equation for $\langle |A|^2 \rangle$ numerically. Our approximation is seen to yield a result much closer to the correct behaviour than the decoupling approximation. For the ramp in $Q(t)$ no numerical solution is available and the accuracy of our approximation is not known precisely, though we expect it to be reasonably good, at least when the ramp is not too slow.

The results of stochastic fits to the data are shown in figures 11 and 12 for the same runs as in figures 2 and 3. The fitting parameter is the strength of the external force $\bar{F}$, which once again determines the time scale for the onset of convection. The quantity $\tilde{g}$, (4.18), which determines the saturation value of $\langle \bar{A}^2 \rangle$ at long times corresponds to that used in the deterministic equation for the intermediate state. It is evident from the solid curve in figure 11 that the stochastic model yields a worse fit to the step data than the deterministic equation. A different value of the external force $\bar{F}$ would shift the curve parallel to the time axis, but would not improve the quality of the fit. For the ramp data shown in figure 12, on the other hand, we obtain a fit with rolls or hexagons (curves *a* and *b*, respectively), which is as good as the deterministic fit in figure 5. [Presumably, putting rolls and hexagons together, as in figure 5, would also work well in this case, but the coupled stochastic equations are rather unwieldy, as mentioned earlier.] We have tested the stochastic theory on data at a higher ramp rate [$\beta = 0{\cdot}2$], and find rather good agreement for short times, using the *same* external force $\bar{F}$ as in figure 12. We conclude from this analysis that the ramp experiments do not distinguish

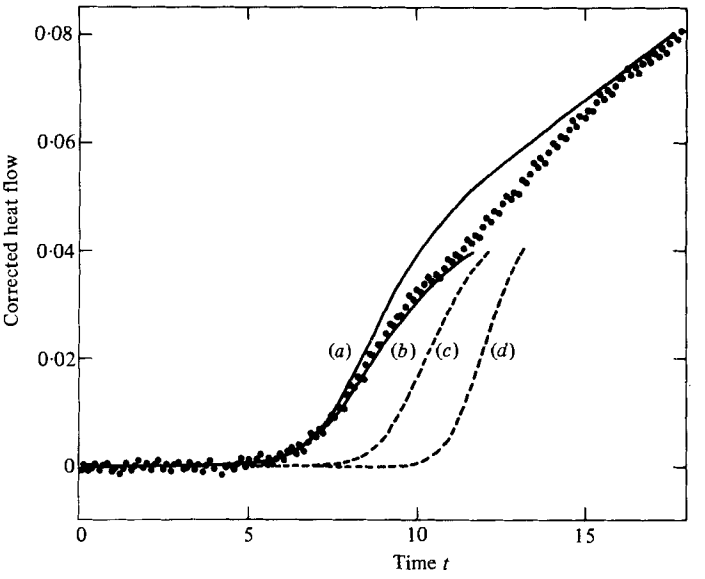

FIGURE 12. The same data as in figure 3, along with a stochastic fit with rolls (curve (*a*)) and hexagons (curve (*b*)). The noise strength $\bar{F} = \eta \bar{F}_{\text{th}}$ is adjusted to the value $\eta = 6 \times 10^3$ for curves (*a*) and (*b*). The dashed curves show a hexagon fit with $\eta = 10^2$ (curve (*c*)) and $\eta = 1$ (curve (*d*)). $\beta = 0{\cdot}01$.

between stochastic and deterministic mechanisms, whereas the step experiments distinctly favour a deterministic model.

Apart from fitting the detailed shape of the $\mathcal{N}(t)$ curve, it is interesting to note the order of magnitude of the noise required to obtain the experimental onset time, and to compare this noise amplitude with that obtained from microscopic thermal fluctuations as given by (2.34). Such a comparison is shown in curves (*c*) and (*d*) of figure 12, which correspond to

$$\bar{F} = \eta \bar{F}_{\text{th}}, \tag{4.22}$$

with $\eta = 10^2$ and 1, respectively, whereas the experimental points are fitted by $\eta = 6 \times 10^3$. (The solid curve in figure 11 also has the value $\eta = 6 \times 10^3$.) It is apparent from curve *d* of figure 12 that the present experiments could detect the effect of the tiny thermal fluctuations ($\eta = 1$) in an accessible time, if there were no other mechanism, stochastic or deterministic, to bring about convective onset earlier.

4.6. *Discussion of results*

In order to gain further insight into the nature of the forcing mechanism, we have studied the dependence of the deterministic forcing parameter $\bar{f}$ on the ramp rate β, over a range of ramp rates. These include values of β for which the theory is not quantitatively valid at large times (see figure 8), but the parameter $\bar{f}$ still determines the onset time for convection, and is rather insensitive to the later evolution. The results obtained from a deterministic fit are presented in figure 13, and show roughly a linear variation of $\bar{f}$ with β

$$\bar{f} = \bar{f}^0 + \bar{f}^1 \beta, \tag{4.23}$$

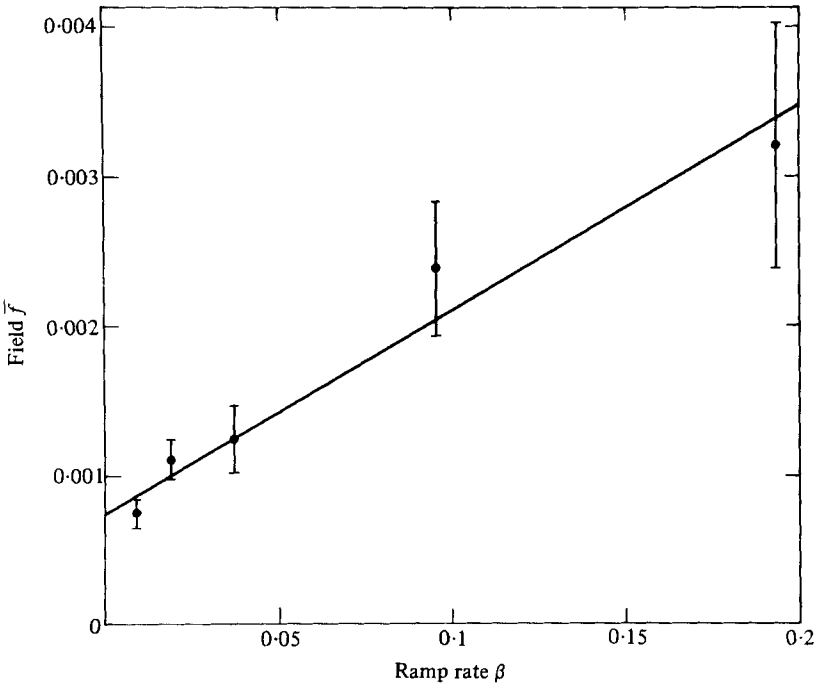

FIGURE 13. The field strength $\bar{f}$ for the deterministic fit as a function of ramp rate. The error bars are estimates of the change in field needed to give a significantly worse fit to the onset. The straight line is given by $\bar{f} = 1{\cdot}4 \times 10^{-2}\beta + 7 \times 10^{-3}$.

with a finite intercept at $\beta = 0$. This dependence may be interpreted by identifying two different contributions to the force $\bar{f}$, one present in the system at all times, and one associated with the time dependence of the external temperature, or Rayleigh number. This interpretation was tested by using (4.23) obtained from the ramp experiments, to fit the step data in the following way. The value of the force in (4.3) was chosen as

$$\bar{f}(t) = \bar{f}^0 + \bar{f}^1 d\bar{\epsilon}/dt, \tag{4.24}$$

and (4.3) and (4.5) were then solved self-consistently for step experiments, without further adjustments. This choice gave an excellent fit to the onset times for all runs, whereas simply using $\bar{f} = \bar{f}^0$, or some average value independent of step size, did not.

The part of the forcing which is associated with the time dependence, namely the term $\bar{f}^1$ in (4.23), can be roughly estimated from a simple calculation using the linearized theory. This estimate is carried out in appendix C, where we find

$$\bar{f}^1 = 0{\cdot}02, \tag{4.25}$$

compared with the experimental value in figure 13 of $\bar{f}^1 = 0{\cdot}014$. The agreement is satisfactory in view of the considerable uncertainties in both estimates.

According to the above picture, if the term $\bar{f}^0$ is present at all times, it should also affect the static results. We thus have an 'imperfect bifurcation' (Kelly & Pal 1976; Daniels 1977; Hall & Walton 1977; Matkowsky & Reiss 1977), and there should be some rounding in the static Nusselt-number data. The time-independent solution of

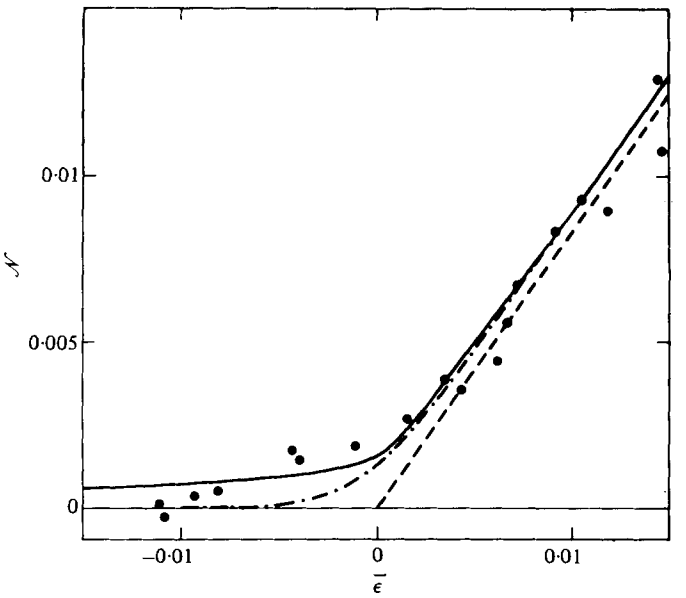

FIGURE 14. The static data of Behringer & Ahlers (1982) for convective heat flow $\mathcal{N} = (N-1)R/R_c$ *vs.* reduced Rayleigh number $\bar{\epsilon} = [R-R_c(L)]/R_c(L)$, in the immediate vicinity of onset (solid points). The solid line is the fluctuation rounded value, equation (D 30), using the noise strength $\bar{F} = 6 \times 10^3 \bar{F}_{\rm th}$ obtained from the onset time. The dash-dotted line is the corresponding deterministic estimate, equation (4.3), with $\bar{f} = \bar{f}^0 = 7 \times 10^{-3}$ coming from the intercept in figure 13. The dashed line is the unrounded (ideal) curve given by $\mathcal{N} = 0{\cdot}84\bar{\epsilon}$.

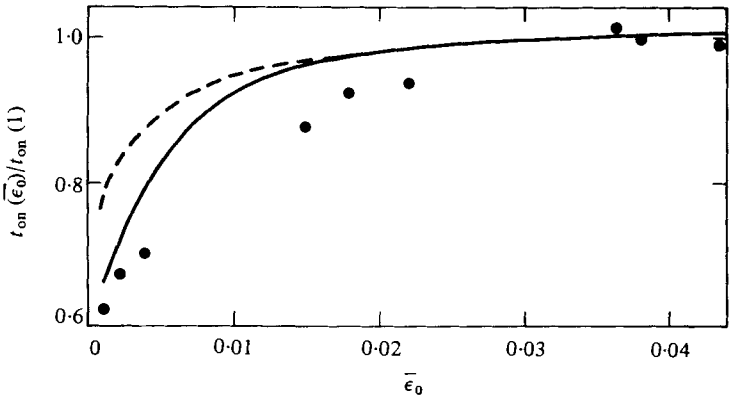

FIGURE 15. The onset time (solid points), as a function of initial steady-state Rayleigh number $\bar{\epsilon} = -\bar{\epsilon}_0$, for the ramp rate of figure 7. The solid line is the result of the deterministic theory, while the dashed line is the stochastic value, $\beta = 0{\cdot}02$.

(4.3) with $\bar{f} = \bar{f}^0$ is shown in figure 14, along with the static data of Behringer & Ahlers (1982) very near R_c. We also show the static rounding predicted by the stochastic theory (see appendix D) using the full $\bar{F} = 6 \times 10^3 F_{\rm th}$ obtained from the dynamic fits. It is apparent from the figure that the experimental rounding is consistent with either description of the dynamic onset. (Note that the absolute magnitude of the fields depends sensitively on the parameter $\bar{\tau}_0$, and is thus uncertain by roughly a factor of 2).

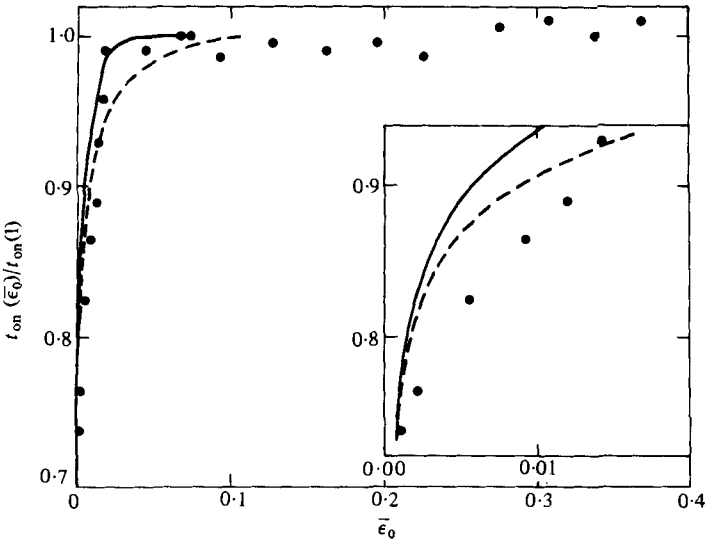

FIGURE 16. The same plot as in figure 15 for a high ramp rate, $\beta = 0{\cdot}2$.

Another way to represent the dynamic data is to define an 'onset time' t_{on} (Foster 1965*a*, *b*), and to study its variation with the parameters in the system. Among the various possible definitions of this time, we have chosen a purely empirical one, namely the time obtained by extrapolating the $\mathcal{N}(t)$ curve back linearly from its inflection point (see figure 8). It is clear that the onset time will depend critically on the initial value of $\bar{A}(t)$, which according to (4.3) depends on the particular Rayleigh number at which the system equilibrated before the time dependence set in. Thus, a number of runs were made with the same ramp rate, but with initial steady states at different values of the Rayleigh number $\bar{\epsilon} = -\bar{\epsilon}_0$, below the threshold. The corresponding onset times are plotted as a function of $\bar{\epsilon}_0$ for two different ramp rates in figures 15 and 16, and compared with the theory. We may first note that both the deterministic and the stochastic theory correctly predict that the onset time becomes shorter as $\bar{\epsilon}_0$ becomes smaller, thus confirming the idea that a 'field' f is present in (2.31), even in the absence of any time dependence. Indeed, for a constant $\bar{\epsilon} = -\bar{\epsilon}_0 < 0$, with $\bar{f} = \bar{f}^0 = \text{const.}$, we have

$$\bar{A}^2 = (\bar{f}^0 \bar{\tau}_0/\bar{\epsilon}_0)^2 \tag{4.26}$$

in the deterministic model (4.3) and

$$\langle|\bar{A}|^2\rangle = \bar{F}/\bar{\epsilon}_0 \tag{4.27}$$

in the stochastic model, both of which increase with decreasing $\bar{\epsilon}_0$. The theoretical curves in figures 15 and 16 were obtained by using $\bar{F} = 6 \times 10^3 \bar{F}_{th}$ in the stochastic case, and by choosing $\bar{f} = \bar{f}^0$ before the ramp is started and $\bar{f} = \bar{f}^0 + \beta \bar{f}^1$ once the ramp is on, in the deterministic model. The agreement is only semi-quantitative in either case, but it does appear to confirm the basic phenomenological assumption contained in (2.31).

Finally, we also show in figure 17 the onset times as a function of ramp rate for all the ramps we considered (choosing values of $\bar{\epsilon}_0$ large enough so that t_{on} is independent of $\bar{\epsilon}_0$). Experimental points are presented for cells A and B, with aspect ratios $L = 4{\cdot}72$ and $L = 2{\cdot}08$, respectively, along with the theoretical predictions from the stochastic theory, using a noise value $\bar{F}$ independent of ramp rate. We may also test the assump-

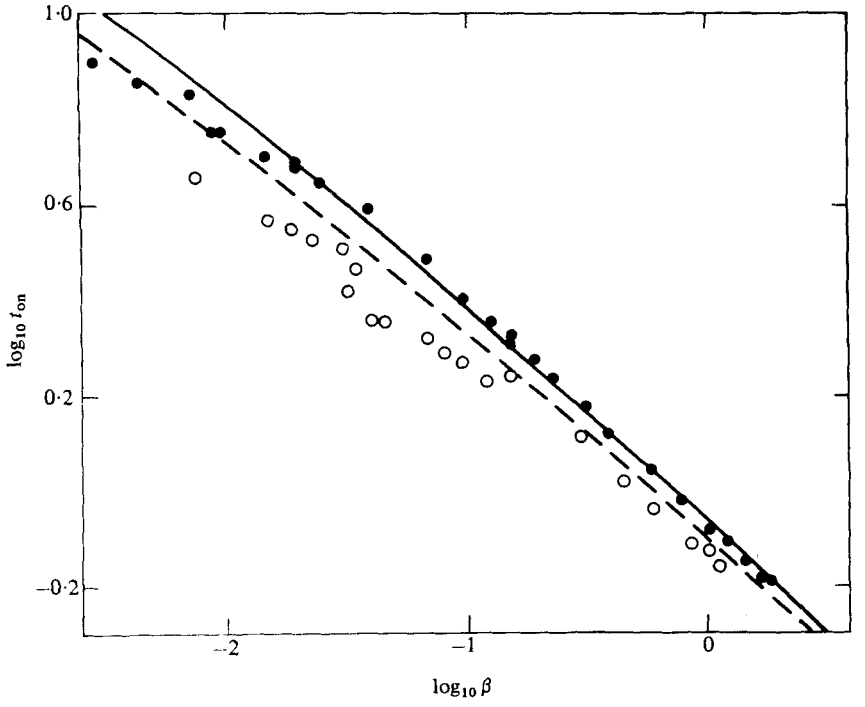

FIGURE 17. The onset time t_{on} *vs.* the ramp rate β on a log–log scale. The solid points are for the cell of reduced radius (aspect ratio) $L = 4{\cdot}72$ (cell A), while the open points are for a cell with $L = 2{\cdot}08$ (cell B). The solid line is the stochastic prediction using $\bar{F} = 6 \times 10^3 \bar{F}_{th}$, for $L = 4{\cdot}72$, independent of ramp rate, while the dashed line is the corresponding prediction for $L = 2{\cdot}08$, with $\bar{F}_{th}$ multiplied by $(4{\cdot}72/2{\cdot}08)^2$ [equation (D 19)].

tion that for different aspect ratios the values of $\bar{F}$ scale as L^{-2}, as predicted in (D 19). Although the experiments extend to ramp rates which immediately carry the system beyond the range of strict validity of the theory, the general consistency of the data with our simple model is reassuring. A similar plot for the deterministic theory with a constant field $\bar{f}$ would give analogous results, since the log–log scale does not resolve the small differences implied by the β dependence of $\bar{f}$ shown in figure 13.

In figure 18 the same experimental results are presented, along with those of Foster (1965*b*), at ramp rates several orders of magnitude higher than the present ones. The onset time is roughly proportional to $\beta^{-\frac{1}{2}}$ for our data, as one would expect from the linearized amplitude equation

$$\bar{A}(t) \sim \bar{A}_0 \exp(\tfrac{1}{2}\beta t^2) \sim \bar{A}_0 \exp(t/t_{on})^2. \tag{4.28}$$

For the higher ramp rates used by Foster, the dependence seems closer to $\beta^{-\frac{2}{3}}$, as one would expect if the onset time in dimensional units were independent of the height d (Foster 1965*a*).

The authors are indebted to N. Schryer for making his partial differential equation program available to them, and for advice on its use. They also wish to thank R. P. Behringer for useful discussion and to acknowledge his contributions to the early stages of the experiment. The research of GA done at UCSB was supported by NSF grant no. DMR 7923289.

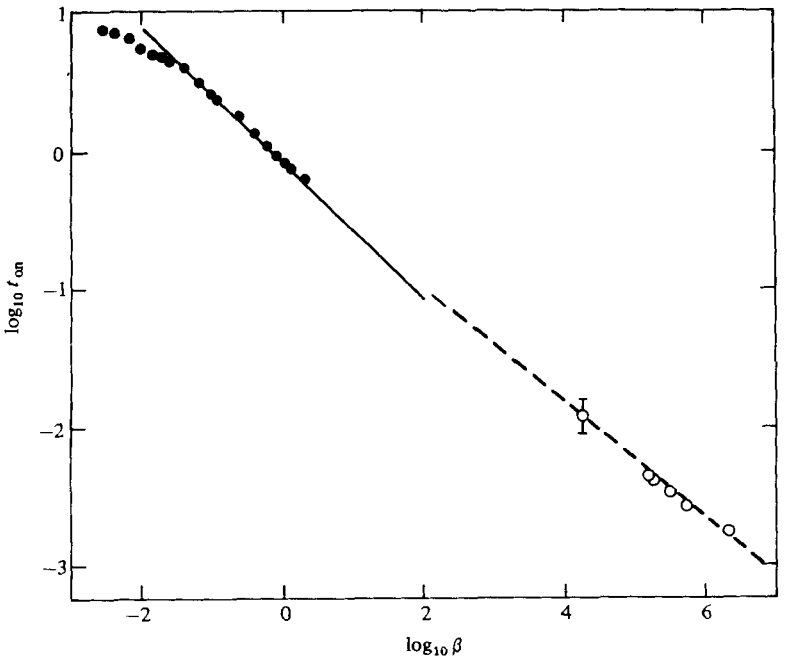

FIGURE 18. The onset time *vs.* β on a larger scale than in figure 17. The solid points are the same as in figure 17, and the open points are taken from the data of Foster (1965*a*) at higher ramp rates. The solid line has slope $-\frac{1}{2}$, while the dashed line has slope $-\frac{2}{3}$.

Appendix A. Summary of amplitude equation

The hydrodynamic equations of motion for the velocity field $(u, v, w) \equiv (\mathbf{u}, w)$ and the deviation θ of the temperature from the linear conduction profile between boundaries at $z = 0$ and 1 are the Oberbeck–Boussinesq equations

$$\dot{\mathbf{u}} = \sigma\left[\nabla^2 + \frac{\partial^2}{\partial z^2}\right]\mathbf{u} - \left[w\frac{\partial}{\partial z} + \mathbf{u}.\nabla\right]\mathbf{u} - \nabla P, \tag{A 1}$$

$$\dot{w} = \sigma\theta + \sigma\left[\nabla^2 + \frac{\partial^2}{\partial z^2}\right]w - \left[w\frac{\partial}{\partial z} + \mathbf{u}.\nabla\right]w - \frac{\partial P}{\partial z}, \tag{A 2}$$

$$\dot{\theta} = Rw + \left[\nabla^2 + \frac{\partial^2}{\partial z^2}\right]\theta - \left[w\frac{\partial}{\partial z} + \mathbf{u}.\nabla\right]\theta, \tag{A 3}$$

$$\nabla.\mathbf{u} + \frac{\partial w}{\partial z} = 0, \tag{A 4}$$

where distance, time and temperature are scaled by d, d^2/κ, and $\kappa\nu/\alpha g d^3$, respectively, the Prandtl number is

$$\sigma = \nu/\kappa, \tag{A 5}$$

and the Rayleigh number is

$$R = \frac{(T_l - T_u)\, g\alpha d^3}{\kappa\nu}. \tag{A 6}$$

The gradient ∇ refers to the two-dimensional horizontal co-ordinate $\mathbf{r}$. We introduce the four-component vector

$$\mathbf{V}(\mathbf{r},z,t) \equiv \begin{pmatrix} u(\mathbf{r},z,t) \\ v(\mathbf{r},z,t) \\ w(\mathbf{r},z,t) \\ \theta(\mathbf{r},z,t) \end{pmatrix} = \begin{pmatrix} \mathbf{u}(\mathbf{r},z,t) \\ w(\mathbf{r},z,t) \\ \theta(\mathbf{r},z,t) \end{pmatrix}, \tag{A 7}$$

and expand this vector in the complete set of eigenfunctions of the system obtained by *linearizing* equations (A 1)–(A 4) (Cross 1980):

$$\mathbf{V}(\mathbf{r},z,t) = \sum_{\mathbf{q},\,i} V_{\mathbf{q}}^{(i)}(t)\,\mathbf{e}_{\mathbf{q}}^{(i)}(\mathbf{r},z). \tag{A 8}$$

The essential approximation involved in the derivation of the amplitude equation is a truncation of the expansion (A 8) to retain only the lowest mode ($i = 1$) and to limit the horizontal wavevectors $\mathbf{q}$ to the vicinity of the circle $|\mathbf{q}| = q_0$, where $\mathbf{q}_0$ is the critical wavevector for convective onset. Thus equation (A 8) becomes

$$\mathbf{V}(\mathbf{r},z,t) = \sum_{|\mathbf{q}|\approx q_0} \mathbf{V}_{\mathbf{q}}^{(1)}(t)\,\mathbf{e}_{\mathbf{q}}^{(1)}(\mathbf{r},z). \tag{A 9}$$

The critical eigenvector $\mathbf{e}^{(1)}$ is written in the form

$$\mathbf{e}_{\mathbf{q}}^{(1)}(\mathbf{r},z) = \frac{1}{\bar{c}} \begin{pmatrix} i\mathbf{q}\bar{u}_0(z) \\ w_0(z) \\ \theta_0(z) \end{pmatrix} e^{i\mathbf{q}.\mathbf{r}}, \tag{A 10}$$

where the functions $\mathbf{u}_0(z) = i\mathbf{q}\bar{u}_0(z)$, $w_0(z)$, $\theta_0(z)$ are the eigenfunctions in the vertical direction, which are equal to

$$u_0(z) = 4i\cos\pi z, \quad w_0(z) = 2\sqrt{2}\sin\pi z, \quad \theta_0(z) = 9\sqrt{2}\,\pi^2\sin\pi z, \tag{A 11}$$

for free boundary conditions. The corresponding expressions for rigid boundary conditions are written down in the appendix of Cross (1980); note, however, that the upper and lower plates are at $z = \pm\frac{1}{2}$ in that work. The quantity $\mathbf{V}_{\mathbf{q}}^{(1)}(t)$ is proportional to the Fourier coefficient of the order parameter

$$\psi_{\mathbf{q}}(t) = c\,V_{\mathbf{q}}^{(1)}(t). \tag{A 12}$$

The constants

$$\bar{c} = [\sigma(\theta_0^2)_m + R_c(|u_0|^2 + w_0^2)_m]^{\frac{1}{2}}, \tag{A 13a}$$

and

$$c = [(w_0\theta_0)_m/R_c]^{\frac{1}{2}}\,\bar{c}^{-1} \tag{A 13b}$$

are determined by the normalization condition (2.4) [the symbol $(\ )_m$ here means an average over the vertical direction]. The $\mathbf{r}$-dependent order parameter is given by

$$\psi(\mathbf{r},t) = \sum_{\mathbf{q}} \psi_{\mathbf{q}}(t)\,e^{i\mathbf{q}.\mathbf{r}}, \tag{A 14}$$

and is a *real* function, since $\psi_{\mathbf{q}} = \psi_{-\mathbf{q}}^*$. The physical variables are

$$\mathbf{V}(\mathbf{r},z,t) = \begin{pmatrix} \mathbf{u}(\mathbf{r},z,t) \\ w(\mathbf{r},z,t) \\ \theta(\mathbf{r},z,t) \end{pmatrix} \approx \frac{1}{c\bar{c}} \begin{pmatrix} \nabla\psi(\mathbf{r},t)\,\bar{u}_0(z) \\ \psi(\mathbf{r},t)\,w_0(z) \\ \psi(\mathbf{r},t)\,\theta_0(z) \end{pmatrix}. \tag{A 15}$$

The amplitude equation (2.5) follows from inserting (A 9) into the hydrodynamic

equations (A 1)–(A 4); the resulting 'free energy' $\mathbf{F}$ is most conveniently written in the $\mathbf{q}$-representation

$$\mathbf{F} = \tfrac{1}{2}\sum_{\mathbf{q}}[-\epsilon+\xi_0^2(q-q_0)^2]\,|\psi_{\mathbf{q}}|^2+\tfrac{1}{4}\sum_{\substack{\mathbf{q}_1,\,\mathbf{q}_2\\ \mathbf{q}_3,\,\mathbf{q}_4}} g(\hat{q}_1\hat{q}_2)\,\psi^*_{\mathbf{q}_1}\psi^*_{\mathbf{q}_2}\psi_{\mathbf{q}_3}\psi_{\mathbf{q}_4}\delta(\mathbf{q}_1+\mathbf{q}_2-\mathbf{q}_3-\mathbf{q}_4). \quad \text{(A 16)}$$

Since the terms quadratic in $\psi_{\mathbf{q}}$ restrict $\mathbf{q}$ values to the region $|\mathbf{q}| = q_0$, the nonlinear coupling g need be calculated only for all $|\mathbf{q}_i| \approx q_0$. Then g is found to be a function of only the angle between $\mathbf{q}_1$ and $\mathbf{q}_2$, which from simple geometrical considerations is the same as the angle between $\mathbf{q}_3$ and $\mathbf{q}_4$, for $\mathbf{q}_1+\mathbf{q}_2 = \mathbf{q}_3+\mathbf{q}_4$ and $|\mathbf{q}_i| = q_0$. The parameters $\tau_0, R_c^\infty, \xi_0$ [see (2.5)] can be calculated explicitly and depend on the boundary conditions on the upper and lower plates. Their values are listed in table 1. The coefficient $g(x)$ is a rather complicated Prandtl-number-dependent function which we do not display here, but refer the reader to Cross (1980).

Given a specific convection pattern (say rolls in the x-direction), we may write the order parameter in terms of the rapidly oscillating term e^{iq_0x}, and a slowly varying *complex* envelope,

$$\psi(\mathbf{r},t) = \sqrt{2}\,\mathrm{Re}\,[A(\mathbf{r},t)\,e^{iq_0x}], \quad \text{(A 17)}$$

where the slow variation of A follows from the restriction $|\mathbf{q}| \approx q_0$ in (A 9). Inserting equations (A 10)–(A 11) into (A 9) we obtain, for instance, the representation of the hydrodynamic variables listed in (2.7) of Newell & Whitehead (1969).

The amplitude equation is given by (2.7) of the text with the coefficient of the nonlinear coupling

$$g = \tfrac{1}{2}g(+1)+g(-1). \quad \text{(A 18)}$$

The values of this expression for rigid–rigid and free–free boundaries are given in table 1.

When the convection pattern is composed of N sets of rolls with specified directions $\hat{q}_i$ one makes the substitution

$$\psi(r,t) = \sqrt{2}\,\mathrm{Re}\Big[\sum_{i=1}^{N} A_i(\mathbf{r},t)\,e^{i\mathbf{q}_i\cdot\mathbf{r}}\Big], \quad \text{(A 19)}$$

with $|\mathbf{q}_i| = q_0$. The form of the amplitude equation derived is (2.11) in the text. Of particular interest for our purposes is a hexagonal pattern composed of three $\mathbf{q}_i$, mutually at an angle $\frac{2}{3}\pi$. The nonlinear coupling coefficients g_{ij} are of two types:

$$\text{diagonal,}\quad g_{11} = \tfrac{1}{2}g(+1)+g(-1), \quad \text{(A 20)}$$

equal to the g defined above; and

$$\text{off diagonal,}\quad g_{12} = g(-1)+g(+\tfrac{1}{2})+g(-\tfrac{1}{2}). \quad \text{(A 21)}$$

Following notation introduced by Newell & Whitehead (1969), we define $g_{12} = g_{11}(1+\bar{\beta})$ so that

$$\bar{\beta} = \frac{g(+\frac{1}{2})+g(-\frac{1}{2})-\frac{1}{2}g(+1)}{\frac{1}{2}g(+1)+g(-1)}. \quad \text{(A 22)}$$

This quantity is also explicitly displayed in table 1. It may be noted that, once the form of the amplitude equation is accepted, the coefficients $\bar{\beta}$ and g can be calculated from results of Schlüter *et al.* (1965) (rigid–rigid) and Pellew & Southwell (1940) (free–free).

Appendix B. Removal of spatial dependence

A single roll pattern

Close enough to onset the shape of the convection pattern is given by the eigenfunction of the linearized differential equation *at* onset. The linear growth rate is the eigenvalue, and the saturation strength is determined by a suitable integral over the nonlinear terms. This, schematically, is how the spatial dependence is removed. The method is best demonstrated by taking a particular example: the cylindrically symmetric state described by (2.20).

The normalized eigenvectors of the linearized form of (2.20), satisfying the boundary conditions, are

$$\phi_n = \sin(n\pi r/L), \tag{B 1}$$

and the scalar product is defined by

$$\langle f_1(r), f_2(r)\rangle = \frac{2}{L}\int_0^L dr f_1(r) f_2(r). \tag{B 2}$$

The amplitude is expanded as

$$A(r) = \sum_{n=1}^{\infty} A_n \phi_n, \tag{B 3}$$

and the convective heat is simply

$$\mathcal{N} = \sum_n |A_n|^2. \tag{B 4}$$

Equation (B 3) is substituted into the differential equation (2.20) and separate equations are derived using the orthogonality of the eigenfunctions,

$$\tau_0 \frac{dA_n}{dt} = (\epsilon - n^2\epsilon_c) A_n - \langle \phi_n, (gL/r)\, \phi_i \phi_j \phi_k\rangle A_i A_j A_k, \tag{B 5}$$

where $\epsilon_c = \pi^2 \xi_0^2/L^2$. This is, in principle, a complete solution of the problem for arbitrary $\epsilon \ll 1$. However for $(\epsilon - \epsilon_c) \ll \epsilon_c$, only A_1 is large (of order $(\epsilon-\epsilon_c)^{\frac{1}{2}}$) with other coefficients A_n, $n \neq 1$, smaller by factors of order $(\epsilon-\epsilon_c)/\epsilon_c$. (Actually, taking into account the strength of the couplings, the expansion parameter is more like $(\epsilon-\epsilon_c)/10\epsilon_c$.) Then the time-dependent $\mathcal{N}$ is given, in fact correct to order $(\epsilon-\epsilon_c)^2$, in terms of the single mode of strength $A_1 \equiv \bar{A}$:

$$\mathcal{N} = \bar{A}^2[1 + O((\epsilon-\epsilon_c)^2)], \tag{B 6}$$

where $\bar{A}$ evolves according to the equation

$$\tau_0 \frac{d\bar{A}}{dt} = [(\epsilon-\epsilon_c) - \bar{g}_4 |\bar{A}|^2 + \bar{g}_6 |\bar{A}|^4]\bar{A}, \tag{B 7}$$

with

$$\bar{g}_4/g = \langle \phi_1, (L/r)\phi_1^3\rangle = 1{\cdot}6595, \tag{B 8}$$

and

$$\frac{\bar{g}_6}{g^2}\epsilon_c = 3\sum_{n=2}^{\infty} \frac{(\langle \phi_n, (L/r)\phi_1^3\rangle)^2}{(n^2-1)} = 0{\cdot}259. \tag{B 9}$$

The terms in $|\bar{A}|^4\bar{A}$ in (B 7) come from the lowest-order coupling to higher-n modes, with the amplitude A_n of these modes calculated to lowest-order as adiabatically

following $\bar{A}$. This is satisfactory only up to this order, and only then can a single-mode description be used. To go to higher orders it is necessary to solve the full system (B 5). From (B 7), neglecting $\bar{g}_6$, one immediately obtains (2.24) of the text.

In deriving (B 7) we assumed that the amplitudes A_n of the modes ϕ_n could be complex numbers since such functions satisfy the boundary conditions (2.21). In fact a more careful analysis shows that the phase is not a free variable, but is fixed by the requirement of finite fluid velocities at the singular point at the centre of the cylinder. This can be seen by comparing the fluid velocities given by the amplitude equation with the velocities in the modes of the linearized hydrodynamic equations (Brown & Stewartson 1978). In the cylindrical geometry we may put the phase factor in the definition of ϕ_n, and assume A to be real. In a rectangular geometry on the other hand, with boundary conditions given by (2.14), a similar analysis would lead to an equation analogous to (B 7), but in this case the full complex equation would have to be used. The phase of A then gives the relative magnitude of the even and odd hydrodynamic modes which go unstable at $\epsilon = \epsilon_c + O(L^{-3})$ (Daniels 1977). The question of whether the amplitude is complex or real is important in our work only in the effect of a stochastic field on the system, treated in appendix D.

Hexagonal pattern

One would like to repeat the procedure for other convection patterns within the cylindrical cell. Unfortunately, without the simplification of cylindrical symmetry, analytic solution even for the linear eigenfunctions seems impossible in finite geometry, and we have resorted to much cruder approximate methods.

Returning to the 'free energy' functional $\tilde{\mathbf{F}}$ (equation (2.2)), we suppose a solution of the form

$$\psi = h(r)\, a(\mathbf{r}), \tag{B 10}$$

where $h(r)$ is a real function assumed cylindrically symmetric, which describes the slow modulation of the amplitude of the convection pattern, forced by the zero boundary condition at the walls; the function $a(\mathbf{r})$ gives the rapid local variation, i.e. the local nature of the convection, analogous to the factor $e^{i\mathbf{q}\cdot\mathbf{r}}$ in (2.9). The amplitude of $a(\mathbf{r})$ is assumed constant over large distances, although it may be necessary to include slowly varying rotations of a basic pattern to conform in some way to the cylindrical boundaries. Equation (B 10) can be looked upon as a variational trial function with parameters to be determined by minimizing the function $\tilde{\mathbf{F}}$.

To describe approximately a pattern of hexagonal cells related to a final cylindrically symmetric roll pattern we have taken

$$h(r) = \frac{1}{r^{\frac{1}{2}}} \sin\frac{\pi r}{L}, \tag{B 11}$$

$$a(\mathbf{r}) \sim \bar{A}_1 e^{iq_0 r} + \bar{A}_2 e^{i\mathbf{q}_2\cdot\mathbf{r}} + \bar{A}_3 e^{i\mathbf{q}_3\cdot\mathbf{r}}, \quad |\mathbf{q}_2| = |\mathbf{q}_3| = q_0, \tag{B 12}$$

where the first term describes a concentric roll pattern, and the next two terms represent rolls locally at an angle $\frac{2}{3}\pi$ to the cylindrical rolls. The amplitudes $|\bar{A}_1|$, $|\bar{A}_2|$ $|\bar{A}_3|$ are assumed spatially constant. Clearly the directions of $\mathbf{q}_1$ and $\mathbf{q}_2$ must vary slowly, in a way which we have not determined, even schematically. However equations (B 11)–(B 12) should provide a reasonable first approximation for an array of hexagonal

cells distorted to accommodate the cylindrical geometry, at least not too close to the centre. Such an ansatz leads to an expression for $\tilde{\mathbf{F}}$ of the form

$$\tilde{\mathbf{F}} \propto (\epsilon-\epsilon_c')\,(|\bar{A}_1|^2+|\bar{A}_2|^2+|\bar{A}_3|^2)-\tfrac{1}{2}\bar{g}_4[|A_1|^4+|A_2|^4+|A_3|^4 + 2\bar{\beta}(|A_1|^2|A_2|^2+|A_2|^2|A_3|^2+|A_3|^2|A_1|^2)], \quad \text{(B 13)}$$

where ϵ_c' is assumed to be roughly the same for all $\bar{A}$'s, and is of order ϵ_c; it arises from the spatial derivatives which depend on the detailed form of $a(\mathbf{r})$. The *overall coefficient* of the nonlinear terms is just determined by $h(r)$, and is the $\bar{g}_4$ calculated above. The *relative strength* of the coupling between rolls is determined only by the *local* structure and it is the $\bar{\beta}$ calculated for infinite geometry, (A 22). Thus minimizing $\tilde{\mathbf{F}}$ with the ansatz, (B 11)–(B 12) leads to the result that for different local patterns (hexagons, squares, rolls, etc.) all slopes $\mathcal{N}/(\epsilon-\epsilon_c')$ in finite geometry are reduced by the same factor $\bar{g}_4/g$ from the laterally infinite values. Moreover, for given geometry, ratios of slopes between different patterns are independent of the geometry. Having found the functional $\tilde{\mathbf{F}}$, we can insert it into (2.1) to find the equation of motion (4.11), used to fit the heating experiments. Note that, in principle, for the hexagonal pattern the expression for $\tilde{\mathbf{F}}$ in (B 13) can contain additional terms proportional to $\mathrm{Re}\,(A_1A_2A_3)$, but their coefficient vanishes for the Boussinesq equations with time-independent driving. Since the coefficients coming from the non-Boussinesq corrections ($Q = -0{\cdot}2$, Busse 1967*a*, *b*; Walden & Ahlers 1981) and from the rate of variation of $\bar{\epsilon}$ (Krishnamurti 1968*a*) are both very small, these lead to no appreciable effect on the predicted time evolution of the amplitude in the present experiments.

Non-cylindrically symmetric roll pattern

Finally, we have also analysed a *linear* roll pattern that breaks the cylindrical symmetry. The centre is no longer a special point, and the amplitude would not be expected to be small there. Therefore we have taken

$$h(r) = \cos\frac{\pi r}{2L}; \quad a(\mathbf{r}) = \bar{A}\,e^{iq_0x}, \quad x = r\cos\theta. \qquad \text{(B 14)}$$

Ignoring derivative terms $\partial^2/\partial y^2$ in (2.20), which lead to terms of higher order in $(\xi_0/L)^2$, we find

$$\mathcal{N} = (1{\cdot}38)^{-1}\,(\epsilon-\bar{\epsilon}_c), \qquad \text{(B 15)}$$

$$\bar{\epsilon}_c = 1{\cdot}18\pi^2\xi_0^2/4L^2. \qquad \text{(B 16)}$$

This yields an onset point *below* that of cylindrical rolls with a node at the centre, $\epsilon_c = (\pi^2\xi_0^2/L^2)$. In fact we can show that the ansatz (B 14) gives a value of $\tilde{\mathbf{F}}$ lower than do cylindrical rolls for all $\epsilon < 38\pi^2\xi_0^2/4L^2$. This implies that the cylindrical rolls are (globally) unstable to a pattern like linear rolls, for a rather wide range of ϵ near onset. A hexagonal pattern based on straight rolls as in (B 14) will also lead to an expression of the form (B 13).

Cylindrical rolls with finite amplitude at the centre

For finite cylinder radius the zero boundary condition at the centre (2.16) is no longer strictly valid, and the possibility exists of a non-zero amplitude at this point.

Such a state has $h = \cos(\pi r/2L)/r^{\frac{1}{2}}$, $a = A\,e^{iq_0 r}$, and a threshold which is again lower than for the state with a node at the centre

$$(\epsilon_{c2} = \pi^2\xi_0^2/4L^2 \quad \text{rather than} \quad \epsilon_c = \epsilon_{c1} = \pi^2\xi_0^2/L^2).$$

The slope of $\mathcal{N}$ *vs.* $\bar{\epsilon}$ as calculated by Brown & Stewartson (1979) for free–free boundary conditions in the limit $L \to \infty$, is equal to $(\bar{g}_4)^{-1} = (2g \ln L)^{-1} = 0{\cdot}46$, for our cell. The finite-amplitude state in the rigid–rigid case was found numerically by Charlson & Sani (1975), who obtained a slope $(\bar{g}_4)^{-1} = 0{\cdot}47$ for $L = 2{\cdot}25$ and $\sigma = 1$. From the limited information available, it is difficult to rule out the finite-amplitude state conclusively, but it appears to us unlikely that this is the state observed in either the static, or the time-dependent heating experiments.

Appendix C. Derivation of heating equation

Since the heating is time dependent, the conducting temperature T_{cond} is not simply a linear function of the height in the cell, even in the absence of convection. This leads to three effects of interest.

(i) The heat conducted from the lower plate is no longer simply proportional to R, so that in the heat balance equation,

$$\begin{pmatrix}\text{heat applied to}\\ \text{lower plate}\end{pmatrix} = \begin{pmatrix}\text{heat conducted from lower}\\ \text{plate (no convection)}\end{pmatrix} + \begin{pmatrix}\text{extra heat due to}\\ \text{convection}\end{pmatrix}, \tag{C 1}$$

there are corrections in the first term on the right-hand side.

(ii) The 'effective Rayleigh number' driving convection is not $R \propto T_l - T_u$. Instead, a weighted average of T_{cond} (with the weighting given by the shape function $w_0(z)\,\theta_0(z)$ of appendix A) must be used. It turns out that these corrections are small, and will be neglected.

(iii) In general the conducting profile will have radial derivatives. The hydrodynamic equations are now incompatible with zero fluid velocities. Thus time-dependent heating acts as a field driving the convection.

To calculate these effects we write an equation for $\theta_c(z, r)$, the deviation of the conducting-temperature profile from the linear interpolation between the instantaneous temperatures T_u of the top and $T_l(t)$ of the bottom plates,

$$T_{\text{cond}}(z, r) = \theta_c(z, r) + T_l(t) + z[T_u - T_l(t)], \tag{C 2}$$

where θ_c is calculated in the absence of convection, and so satisfies the equation

$$\frac{\partial \theta_c}{\partial t} - \nabla^2 \theta_c = -\frac{dT_l}{dt}(1 - z), \tag{C 3}$$

where the dimensionless quantities of appendix A are used. Since for $\epsilon \ll 1$ convection gives a small perturbation to the total heat flow, the solution for θ_c may continue to be be used above onset. Equation (C 3) is readily solved in an approximation in which θ_c follows the driving term adiabatically, i.e. $\partial\theta_c/\partial t$ is neglected. It can be shown that this corresponds to the first term in an expansion in $\pi^{-2}\,\partial/\partial t \approx 0{\cdot}002$ for typical ramp

rates used. Assuming good conductors for the lateral boundaries (i.e. $\theta_c = 0$ for $r = L$) this gives

$$\theta_c = -\frac{dT_l}{dt} \sum_{n,s} \frac{2}{n\pi} \frac{2}{\pi\beta_{os} J_1(\pi\beta_{os})} \frac{1}{\pi^2[n^2 + (\beta_{os}/L)^2]} \sin(n\pi z) J_0(\pi\beta_{os} r/L), \tag{C 4}$$

where β_{os} is defined by $J_0(\pi\beta_{os}) = 0$.

The heat conducted from the bottom plate is proportional to $-(\partial T_{\text{cond}}/\partial z)_{z=0}$ averaged over the plate. Evaluating the contribution due to θ_c from (C 4) numerically for $L = 4{\cdot}7$ gives for this average

$$\left\langle \left(-\frac{\partial T_{\text{cond}}}{\partial z} \right)_{z=0} \right\rangle = (T_l(t) - T_u) + 0{\cdot}30 \frac{\partial T_l(t)}{\partial t}. \tag{C 5}$$

The heat conducted from the bottom plate through the liquid is thus equal to

$$\bar{Q}_{\text{liquid}} = 1 + \bar{\epsilon} + 0{\cdot}30\, d\bar{\epsilon}/dt, \tag{C 6}$$

where we have normalized by the corresponding value for a *static* temperature difference at $\bar{\epsilon} = 0$. In addition there is a contribution from conduction through the cell walls, to give for the total heat conducted from the lower plate

$$\bar{Q} = (1 + \lambda_w)(1 + \bar{\epsilon}) + 0{\cdot}30\, d\bar{\epsilon}/dt. \tag{C 7}$$

with $\lambda_w = 2(\bar{t}/L)(K_w/K_l) = 0{\cdot}14$ in the present experiments for cell A, where $\bar{t}$ is the thickness of the wall and K_w/K_l the ratio of the thermal conductivities of the wall and liquid. Finally it is convenient to subtract from $\bar{Q}$ its values $\bar{Q}_c$, for $\bar{\epsilon} \equiv 0$ and $d\bar{\epsilon}/dt = 0$, to give a quantity we call the heat flow Q:

$$Q \equiv \bar{Q} - \bar{Q}_c = (1 + \lambda_w)\bar{\epsilon} + 0{\cdot}30\, d\bar{\epsilon}/dt. \tag{C 8}$$

The numerical coefficient in front of $d\bar{\epsilon}/dt$ depends on the assumption of perfectly conducting walls–insulating walls would instead give a coefficient $\frac{1}{3}(1 + \lambda_w)$. In addition any thermal mass attached to the lower plate would act to increase this coefficient. [In practice we believe there is a correction from this effect.] Thus the coefficient is best evaluated from experiment, for example from the change in $\bar{\epsilon}$ when the ramp is turned on, well below onset; the value obtained in our cell was 0·5. In equations (4.1)–(4.2) we have denoted this coefficient by c_1.

Above onset there is an additional contribution to the heat flow from convection. By our choice of normalization this is simply $\mathcal{N}$, so that above onset we have

$$Q = (1 + \lambda_w)\bar{\epsilon} + c_1 \frac{d\bar{\epsilon}}{dt} + \mathcal{N}. \tag{C 9}$$

The experimentally accessible quantities are $Q(t)$ and $\bar{\epsilon}(t)$. The interesting quantity theoretically is $\mathcal{N}(t)$. To compare theory with experiment we wish to plot a quantity which is directly measured, but displays the behaviour of $\mathcal{N}$. The convenient choice, which we call the 'corrected heat flow', is slightly different for the steps and ramps. For the steps it is

$$\text{corrected heat flow} = Q - (1 + \lambda_w)\bar{\epsilon} = \mathcal{N} + c_1 \frac{d\bar{\epsilon}}{dt}. \tag{C 10}$$

Notice that this quantity reduces to $\mathcal{N}$ when $d\bar{\epsilon}/dt = 0$, but it will have large corrections

at small times, just after the step is applied. For the ramps we make an additional subtraction, so that the quantity plotted passes through zero when $\mathcal{N}$ is zero, i.e. we write:

$$\text{corrected heat flow} = Q - (1+\lambda_w)\,\bar{\epsilon} - c_1\beta = \mathcal{N} + c_1\left(\frac{d\bar{\epsilon}}{dt} - \beta\right), \tag{C 11}$$

where β is the ramp rate. In either case we have two expressions for the corrected heat flow, one involving purely experimental quantities, the other to be calculated from theory. These are the quantities plotted in the figures.

Finally we should point out here that experimentally the steps and ramps are applied to the heat input to the lower plate, equal to Q. After initial transients have died out, but before convection begins, $\bar{\epsilon}$ will correspondingly have been stepped, or will be following a ramp. Since it is $\bar{\epsilon} \neq 0$ that drives convection, we have quoted the steps and ramps in $\bar{\epsilon}$, rather than those in Q, in describing the fits to experiment. As seen from (C 9), the changes in $\bar{\epsilon}$ are related to corresponding changes in Q by the factor $(1+\lambda_w)$, e.g. for the ramp rate we quote β given by

$$\beta = \gamma/(1+\lambda_w), \tag{C 12}$$

where γ is the applied heat ramp dQ/dt, (3.2*b*).

In order to estimate the strength of the driving term mentioned in (iii) above, we isolate the radial dependence in the equation for the velocity w [equation (A 2)], i.e.

$$\dot{w} \sim \sigma T_{\text{cond}}(\mathbf{r}, z), \tag{C 13}$$

where $T_{\text{cond}}(\mathbf{r}, z)$ is the conducting profile. We wish to project this equation onto the order parameter $\psi(\mathbf{r})$, i.e. on the lowest eigenvector $\mathbf{e}^{(1)}$, equation (A 9). Let us write

$$\dot{V}_q^{(1)} = \langle \mathbf{e}_q^{(1)}, (0, 0, \sigma T_{\text{cond}}) \rangle \tag{C 14}$$

$$= \frac{1}{\bar{c}_q} \int dz \int d^2r\, \sigma R_c w_q^*\, T_{\text{cond}}(r, z), \tag{C 15}$$

$$\bar{c}_q^2 \equiv \int dz \int d^2r [\sigma\,|\theta_q|^2 + R_c(|u_q|^2 + |w_q|^2)]. \tag{C 16}$$

(Note that the contribution from the pressure term in (A 2) drops out in forming the scalar product). According to Schlüter *et al.* (1965) we may write

$$w_q^* = e^{-i\mathbf{q}\cdot\mathbf{r}} q^2 f_q(z), \tag{C 17}$$

with $f_q(z) \to$ const. as $q \to 0$, so we may integrate by parts in (C 15) to obtain

$$\psi_q = -(c/\bar{c}_q) \int dz \int d^2r\, \sigma R_c f_q(z) [\nabla_r^2 T_{\text{cond}}(r, z)]\, e^{-i\mathbf{q}\cdot\mathbf{r}}, \tag{C 18}$$

where c is defined in (A 13*b*). For the case of free–free boundary conditions

$$\bar{f}(z) \equiv (\sigma R_c/\bar{c}_q) f_q(z) \tag{C 19}$$

is independent of q; if we assume the same for the rigid–rigid case we find

$$\psi(r) = -\,c \int dz \bar{f}(z)\, \nabla_r^2 T_{\text{cond}}(z, r). \tag{C 20}$$

For a cylindrical system, we wish to project equation (C 20) along the $n = 1$ mode of the amplitude expansion (B 3). Using the expressions (C 3)–(C 4) for T_{cond}, a rough estimate of the integrals leads to

$$\dot{A} = 0{\cdot}02\, d\bar{\epsilon}/dt, \tag{C 21}$$

as quoted in (4.25).

Appendix D. Stochastic equation

Let us consider the nonlinear stochastic equation

$$\dot{A} = \tau_0^{-1}[\epsilon(t) - gA^2]A(t) + f(t), \tag{D 1}$$

where the force f is a Gaussian random variable with mean zero and a white-noise spectrum

$$\langle f(t)f(t')\rangle = 2\tau_0^{-1}\bar{F}\delta(t-t'), \tag{D 2}$$

and for simplicity the variable $A(t)$ is taken to be real. We wish to calculate $\langle A^2(t)\rangle$ for a specified form of $\epsilon(t)$, in the limit of weak noise, $[\bar{F} \to 0]$, when the system starts near an unstable position $A = 0$. This problem has recently been considered by Suzuki (1978), Haake (1978) and de Pasquale & Tombesi (1979), for a time independent $\epsilon(t)$, with some specified initial probability distribution, e.g. $P(A, 0) = \delta(A)$. We wish to generalize this treatment to an arbitrary time-dependent $\epsilon(t)$. To do this we write down the solution of the *deterministic* equation ($f = 0$), with initial value A_0 at $t = 0$,

$$A^2(t) \equiv \frac{R_1^2(t)\,A_0^2}{1 + R_2(t)\,A_0^2}, \tag{D 3}$$

where

$$R_1(t) = \exp\left[\tau_0^{-1}\int_0^t \epsilon(s)\,ds\right], \tag{D 4}$$

$$R_2(t) = 2g\tau_0^{-1}\int_0^t R_1^2(s)\,ds. \tag{D 5}$$

Equation (D 3) may be used in the stochastic case ($f \neq 0$) to *define* the variable $A_0(t)$, which satisfies the stochastic equation

$$\dot{A}_0 = f(t)\,R_1^{-1}(t)\,[1 + A_0^2(t)\,R_2(t)]^{\frac{3}{2}}, \tag{D 6}$$

with no drift, but a more complicated noise. We now make the approximation, valid at short times, of linearizing (D 6), which turns A_0 into a Gaussian variable with probability distribution

$$P_0(A_0, t) = [2\pi\tilde{A}^2(t)]^{-\frac{1}{2}}\exp[-A_0^2/2\tilde{A}^2(t)], \tag{D 7}$$

$$\tilde{A}^2(t) = \tilde{A}_0^2 + 2\bar{F}\tau_0^{-1}\int_0^t R_1^{-2}(s)\,ds. \tag{D 8}$$

$$\tilde{A}_0^2 \equiv \int_{-\infty}^{\infty} dx\,x^2\,P_0(x, 0). \tag{D 9}$$

The corresponding expression for $A(t)$ is obtained by using (D 3) and (D 7), from which we find

$$\langle A^2(t)\rangle = A_s^2(t)\int_{-\infty}^{\infty}\frac{d\xi}{\sqrt{(2\pi)}}\left[\frac{\xi^2\tau(t)}{1+\xi^2\tau(t)}\right]e^{-\frac{1}{2}\xi^2}, \tag{D 10}$$

$$A_s^2(t) \equiv R_1^2(t)/R_2(t), \tag{D 11}$$

$$\tau(t) \equiv \tilde{A}^2(t)\,R_2(t). \tag{D 12}$$

At large times it may be verified that $\tau(t) \to \infty$, so $\langle A^2\rangle = A_s^2$, which is the large time

behaviour of the deterministic solution (D 3). Thus our approximation (D 10) interpolates between the correct behaviour at short and long times. For a constant $\epsilon(t)$, the approximation essentially agrees with those of Suzuki (1978), Haake (1978), and de Pasquale & Tombesi (1979), and also with the numerical solution by Jhaveri & Homsy (1980) mentioned in the text (figure 10).

In applying the above method to a solution of (D 1), we shall use a function $\epsilon(t)$ which is a constant $-\epsilon_0$ for $t < 0$, and at $t = 0$ either jumps to a finite positive value ϵ_1, or has a linear dependence on time. The distribution of A^2 at $t = 0^-$ is a Gaussian with variance $\tilde{A}_0^2$, and it can be calculated by linearizing (D 1), since there is no instability as long as $\epsilon(t) < 0$. The value obtained is

$$\langle A^2 \rangle = \tilde{A}_0^2 = \overline{F}/\epsilon_0. \tag{D 13}$$

Equations (D 10)–(D 13) provide a complete (approximate) solution of the stochastic equation (D 1).

Let us now turn to an estimate of the noise parameter $F = F_{\text{th}}$ in (2.33), arising from thermal fluctuations on a molecular level. Correlation functions of hydrodynamic variables below the Rayleigh–Bénard threshold ($\epsilon = -\epsilon_0$), have been estimated on the basis of the linear theory, by Zaitsev & Shliomis (1970), Graham (1974) and Swift & Hohenberg (1977). The results are

$$\langle \theta(\mathbf{q})\, w(\mathbf{q}') \rangle = (2\pi)^2 \delta(\mathbf{q}+\mathbf{q}')\, X_{\theta w}[\epsilon_0 + \xi_0^2 (q^2 - q_0^2)^2/4q_0^2]^{-1},$$

$$X_{\theta w} \equiv \left(\frac{k_B T}{\rho}\right)^{\frac{1}{2}} \left(\frac{k_B T^2}{c_v}\right)^{\frac{1}{2}} \left[\frac{\sigma \tilde{\gamma}^{\frac{1}{2}}}{1+\sigma}\right] [1 + (\tilde{\gamma}\sigma)^{-1}], \tag{D 14}$$

$$\tilde{\gamma} \equiv 3\beta c_v / T\rho g \alpha \sigma \gg 1, \tag{D 15}$$

where c_v is the constant-volume specific heat (per unit volume). The relation between $\psi_{\mathbf{q}}$ and the (dimensionless) hydrodynamic variables implies

$$\langle \psi_{\mathbf{q}} \psi_{\mathbf{q}'} \rangle = \langle w(\mathbf{q})\, \theta(\mathbf{q}') \rangle [d/\kappa(T_l - T_u)]. \tag{D 16}$$

On the other hand, the $\langle \psi\psi \rangle$ correlation function below threshold can be simply calculated from the linearized form of (2.31),

$$\langle \psi_{\mathbf{q}} \psi_{\mathbf{q}'} \rangle = (2\pi)^2 \delta(\mathbf{q}+\mathbf{q}')\, \mathbf{F}[\epsilon_0 + \xi_0^2 (q^2 - q_0^2)^2/4q_0^2]^{-1}. \tag{D 17}$$

Comparison of (D 16) and (D 17) yields

$$F = F_{\text{th}} = \left(\frac{k_B T}{\nu^2 \rho d}\right) \left(\frac{\sigma^2}{1+\sigma}\right) \left(\frac{3}{R_c}\right)^{\frac{1}{2}}, \tag{D 18}$$

where we have neglected the $\tilde{\gamma}\sigma$ term in the last bracket of (D 14). Note that although the calculations were carried out consistently for free–free boundary conditions, we shall apply the final formula to the rigid–rigid case.

In order to estimate the thermal noise field appropriate to the *single-mode* equation (4.17) we must project (2.31) onto the lowest mode of (2.22). It turns out that this merely introduces a factor of the horizontal area of the cell into the noise source, i.e. F in (3.32) and $\overline{F}$ in (4.20) are related by

$$\overline{F} = F/S = F/\pi L^2, \tag{D 19}$$

$$\overline{F}_{\text{th}} = F_{\text{th}}/\pi L^2. \tag{D 20}$$

The static value of the Nusselt number, on the other hand, is related to the local average

$$\langle\psi^2(r)\rangle = \int \frac{d\mathbf{q}}{(2\pi)^2}\int \frac{d\mathbf{q}'}{(2\pi)^2}\langle\psi_{\mathbf{q}}\psi_{\mathbf{q}'}\rangle, \tag{D 21}$$

which involves the higher q modes of (2.22) as well. The calculation of such static averages using the nonlinear equation in two dimensions cannot be carried out exactly, even in the infinite system, but a reasonable self-consistent estimate can be obtained in that case. As discussed, for example, in § VI (*a*) of Graham (1974), $\langle\psi^2\rangle$ below threshold ($\epsilon = -\epsilon_0 < 0$) is given by the solution to the self-consistent equation

$$\langle\psi^2\rangle = F\int \frac{d\mathbf{q}}{(2\pi)^2}[\tilde{\epsilon} + \xi_0^2(q^2 - q_0^2)^2/4q_0^2]^{-1} \tag{D 22}$$

$$= (Fq_0/4\xi_0\tilde{\epsilon}^{\frac{1}{2}})\left[1 + \frac{2}{\pi}\tan^{-1}(\xi_0 q_0/2\tilde{\epsilon}^{\frac{1}{2}})\right], \tag{D 23}$$

$$\tilde{\epsilon} \equiv \epsilon_0 + 3g\langle\psi^2\rangle. \tag{D 24}$$

For $\epsilon = \epsilon_0 > 0$, a reasonable approximation is

$$\langle\psi^2\rangle = \epsilon_0/g + \langle\tilde{\psi}^2\rangle, \tag{D 25}$$

where $\langle\tilde{\psi}^2\rangle$ satisfies (D 22) with (D 24) replaced by

$$\tilde{\epsilon} = 2\epsilon_0 + 3g\langle\tilde{\psi}^2\rangle. \tag{D 26}$$

For $\epsilon_0 = 0$ we obtain

$$\langle\psi^2\rangle = [Fq_0/2\sqrt{3}\xi_0 g^{\frac{1}{2}}]^{\frac{2}{3}}. \tag{D 27}$$

In applying these formulae to the finite system we shall replace ϵ by $\bar{\epsilon}$, so (D 24) becomes

$$\tilde{\epsilon} = -\bar{\epsilon} + 3g\langle\psi^2\rangle, \quad \bar{\epsilon} < 0, \tag{D 28}$$

and (D 26) becomes

$$\tilde{\epsilon} = 2\bar{\epsilon} + 3g\langle\tilde{\psi}^2\rangle, \quad \bar{\epsilon} > 0. \tag{D 29}$$

In addition, the value of $\langle\psi^2\rangle$ above onset in the absence of fluctuations is $\bar{\epsilon}/\bar{g}$ in the finite system so we replace (D 25) by

$$\langle\psi^2\rangle = \bar{\epsilon}/\bar{g} + \langle\tilde{\psi}^2\rangle, \tag{D 30}$$

but retain g in the fluctuation formulae (D 28)–(D 29). Using the enhancement factor η obtained from the dynamic data, we obtain $F = 6\times10^3 F_{\text{th}} = 2{\cdot}16\times10^{-5}$. Thus we estimate the fluctuations at onset ($\bar{\epsilon} = 0$) from (D 27) as

$$\langle\psi^2\rangle = 1{\cdot}53\times10^{-3}, \quad \bar{\epsilon} = 0. \tag{D 31}$$

The values of $\langle\psi^2\rangle$ as a function of $\bar{\epsilon}$ obtained from (D 30) are plotted in figure 14, and agree with the data within the experimental scatter, though the large tail at negative $\bar{\epsilon}$ seems somewhat suspect.

REFERENCES

AHLERS, G. 1978 *Bull. Am. Phys Soc.* **23**, 525.

AHLERS, G. 1980 *J. Fluid Mech.* **98**, 137.

AHLERS, G. & HOHENBERG, P. C. 1978 17*the Int. Solvay Conf. on Physics, Brussels, Belgium.*

AHLERS, G. & WALDEN, R. W. 1980 *Phys. Rev. Lett.* **44**, 445.

BEHRINGER, R. & AHLERS, G. 1977 *Phys. Lett.* A **62**, 329.

BEHRINGER, R. & AHLERS, G. 1982 (To be published).
BROWN, S. N. & STEWARTSON, K. 1977 *SIAM* **57**, 187.
BROWN, S. N. & STEWARTSON, K. 1978 *Proc. Roy. Soc.* A **360**, 455.
BROWN, S. N. & STEWARTSON, K. 1979 *SIAP* (to be published).
BUSSE, F. 1967*a* *J. Math. & Phys.* **46**, 140.
BUSSE, F. 1967*b* *J. Fluid Mech.* **30**, 625.
BUSSE, F. 1978 *Rep. Prog. Phys.* **41**, 1929.
CHARLSON, G. S. & SANI, R. L. 1975 *J. Fluid Mech.* **71**, 209.
CROSS, M. 1980 *Phys. Fluids* **23**, 1727.
CROSS, M., DANIELS, P. G., HOHENBERG, P. C. & SIGGIA, E. D. 1980 *Phys. Rev. Lett.* **45**, 898.
DANIELS, P. G. 1977 *Proc. Roy. Soc.* A **358**, 173.
DAVIS, S. H. 1971 *J. Fluid Mech.* **45**, 33.
FOSTER, T. D. 1965*a* *Phys. Fluids* **8**, 1249.
FOSTER, T. D. 1965*b* *Phys. Fluids* **8**, 1770.
FOSTER, T. D. 1969 *Phys. Fluids* **12**, 2482.
GOLLUB, J. P. & FREILICH, M. H. 1976 *Phys. Fluids* **19**, 618.
GOLLUB, J. P. & BENSON, S. V. 1980 *J. Fluid Mech.* **100**, 449.
GRAHAM, R. 1974 *Phys. Rev.* A **10**, 1762.
HAAKE, F. 1978 *Phys. Rev. Lett.* **41**, 1685.
HALL, P. & WALTON, I. C. 1977 *Proc. Roy. Soc.* A **358**, 199.
HOMSY, G. M. 1973 *J. Fluid Mech.* **60**, 129.
JHAVERI, B. & HOMSY, G. M. 1980 *J. Fluid Mech.* **98**, 329.
JOSEPH, D. D. 1976 *Stability of Fluid Motions.* Springer.
KELLY, R. E. & PAL, D. 1978 *J. Fluid Mech.* **86**, 433.
KOSCHMIEDER, E. L. & PALLAS, S. G. 1974 *Int. J. Heat Mass Transfer* **17**, 991.
KRISHNAMURTI, R. 1968*a* *J. Fluid Mech.* **33**, 445.
KRISHNAMURTI, R. 1968*b* *J. Fluid Mech.* **33**, 457.
LIBCHABER, A. & MAURER, J. 1978 *J. Physique Lett.* **39**, 369.
LICK, W. 1965 *J. Fluid Mech.* **21**, 565.
MATKOWSKI, B. J. & REISS, E. L. 1977 *SIAM J. Appl. Math.* **33**, 230.
MORTON, R. R. 1957 *Quart. J. Mech. Appl. Math.* **10**, 433.
NEWELL, A. C. & WHITEHEAD, J. A. 1969 *J. Fluid Mech.* **38**, 279.
NEWELL, A. C., LANGE, C. G. & AUCOIN, P. J. 1970 *J. Fluid Mech.* **40**, 513.
NORMAND, C., POMEAU, Y. & VELARDE, M. G. 1977 *Rev. Mod. Phys.* **49**, 581.
PASQUALE, F. DE & TOMBESI, P. 1979 *Phys. Lett.* A **72**, 7.
PELLEW, A. & SOUTHWELL, R. V. 1940 *Proc. Roy. Soc.* A **176**, 312.
ROBINSON, J. L. 1967 *J. Fluid Mech.* **29**, 461.
SANO, M. & SAWADA, Y. 1978 *Prog. Theor. Phys.* (*Kyoto*) *Suppl.* **64**, 202.
SCHLÜTER, A., LORTZ, D. & BUSSE, F. 1965 *J. Fluid Mech.* **23**, 129.
SCHRYER, N. 1977 *Bell Laboratories Computing Science Tech. Rep.* 53.
SEGEL, L. A. 1969 *J. Fluid Mech.* **38**, 203.
SHAUMEYER, J. N., BEHRINGER, R. P. & BAIERLEIN, R. 1980 *J. Fluid Mech.* (to be published).
SPANGENBERG, W. G. & ROWLAND, W. R. 1961 *Phys. Fluids* **4**, 743.
STORK, K. & MÜLLER, U. 1975 *J. Fluid Mech.* **71**, 231.
SUZUKI, M. 1978 *Phys. Lett.* A **67**, 339.
SWIFT, J. & HOHENBERG, P. C. 1977 *Phys. Rev.* A **15**, 319.
WALDEN, R. W. & AHLERS, G. 1981 *J. Fluid Mech.* (to be published).
WANKAT, P. C. & HOMSY, G. M. 1977 *Phys. Fluids* **20**, 1200.
WESFREID, J., POMEAU, Y., DUBOIS, M., NORMAND, C. & BERGÉ, P. 1978 *J. Physique Lett.* **39**, 725.
ZAITSEV, V. M. & SHLIOMIS, M. I. 1970 *Zh. Eksp. Teor. Fiz.* **59**, 1583 (also *Sov. Phys., J. Exp. Theor. Phys.* **32**, 866, 1971).